Shear stresses on megathrusts: Implications for mountain building behind subduction zones

Simon Lamb[1]

[1]   Shear stresses τ on a subduction megathrust play an important role in determining the forces available for mountain building adjacent to a subduction zone. In this study, the temperatures and shear stresses on megathrusts in 11 subduction zones around the Pacific rim (Hikurangi, Tonga, Izu-Ogasawara, western Nankai, northeastern Japan, Aleutians, western Alaska, Cascadia, northern Chile, southern Chile) and SE Asia (northern Sumatra) have been determined. The main constraint is that vertical normal stresses beneath the highlands behind the subduction zone are nearly equal to horizontal normal stresses, in the plane of a trench- or arc-normal section. For a typical brittle and ductile megathrust rheology, frictional shear stress $\tau = \mu \rho g z$, for depth z, and ductile shear stress $\tau = A \exp (B/RT)$ at temperature T, where μ, A, B are rheological parameters treated as constants. Rheological constants common to all the megathrusts (μ_{crust}, μ_{mantle}, B) are determined by simultaneously solving for the force balance in the overlying wedge and megathrust thermal structure, using a simplex minimization algorithm, taking account of the induced mantle corner flow at depth (65 ± 15 km (2σ)) and constant radiogenic heating (0.65 ± 0.3 $\mu W\ m^{-3}$ (2σ)) throughout the crust. The A constants are solved individually for each subduction zone, assuming that the maximum depth of interplate slip earthquakes marks the brittle-ductile transition. The best fit solution shows two groupings of megathrusts, with most subduction zones having a low mean shear stress in the range $7-15$ MPa ($\mu_{crust} = 0.032 \pm 0.006$, $\mu_{mantle} = 0.019 \pm 0.004$) and unable to support elevations >2.5 km. For a typical frictional sliding coefficient $\sim$0.5, the low effective coefficients of friction suggest high pore fluid pressures at $\sim$95% lithostatic pressure. Tonga and northern Chile require higher shear stresses with $\mu_{crust} = 0.095 \pm 0.024$, $\mu_{mantle} = 0.026 \pm 0.007$, suggesting slightly lower pore fluid pressures, at $\sim$81% lithostatic. Ductile shear in the crust is poorly resolved but in the mantle appears to show a strong power law dependency, with $B = 36 \pm 18$ kJ mol^{-1}. A_{mantle} values are sensitive to the precise value of B but are in the range $1-20$ kPa. The power law exponent n for mantle flow is poorly constrained but is likely to be large ($n > 4$). The brittle-ductile transition in the crust occurs at temperatures in the range $370°C-512°C$, usually close to the base of the crust and in the mantle at much lower temperatures ($180°C-300°C$), possibly reflecting a marked change in pore fluid pressure or quasi ductile and subfrictional properties. In subduction zones where the subducted slab is older than 50 Ma, a significant proportion of the integrated shear force on the megathrust is taken up where it cuts the mantle and temperatures are $\leq 300°C$. In much younger subduction zones, the stress transmission is confined mainly to the crust. The shear stresses, particularly in the crust, may be kept low by some sort of lubricant such as abundant water-rich trench fill, which lowers the frictional sliding coefficient or effective viscosity and/or raises pore fluid pressure. The unusual high stress subduction zone in northern Chile lacks significant trench fill and may be poorly lubricated, with a mean shear stress $\sim$37 MPa required to support elevations >4 km in the high Andes. However, where the crust is thin in sediment-starved and poorly lubricated subduction zones, such as Tonga, the mean shear stress will still be low. Sediment may

---

[1]Department of Earth Sciences, University of Oxford, Oxford, UK.

lubricate megathrusts accommodating underthrusting of continental crust, such as in the Himalayas or eastern central Andes, which have a low mean shear stress ∼15 MPa.

1. Introduction

[2] Any understanding of the dynamics of continental deformation requires a knowledge of the rheological behavior of the continental lithosphere. Not only is it necessary to consider the effects of temperature and pressure, but also the differences in composition between the crust and mantle. This makes the description of the bulk rheological properties of the lithosphere particularly difficult, and there has been a tendency to focus on either the crust or mantle as the strength determining parts.

[3] Rock mechanic experiments suggest that if the crust is wet, but the mantle is dry, then the strength of the lithosphere will lie mainly in the mantle, and the rheological properties of the lithosphere are essentially those of the mantle [*Ranalli*, 1995; *Hirth and Kohlstedt*, 1996; *Mackwell et al.*, 1998; *Jackson*, 2002]. This has motivated a number of kinematic and dynamical models of continental deformation, in which the brittle crust plays an essentially passive role, deforming in a way that follows most closely the underlying mantle flow [*McKenzie and Jackson*, 1983, 1986; *England and Houseman*, 1986; *Houseman and England*, 1986; *Lamb*, 1987, 1994, 2002]. Such a view has the advantage of providing a tractable way to analyze crustal deformation, and is also consistent with the observation that continental lithosphere often has an elastic thickness many times greater than the crustal thickness [*Watts*, 2001].

[4] It has been argued [*Jackson*, 2002; *Maggi et al.*, 2000a, 2000b; *McKenzie and Fairhead*, 1997] that the long-term elastic strength of the lithosphere lies in the seismogenic zone, which undergoes brittle failure. Thus the discovery from recent improvements in earthquake location [*Jackson*, 2002; *Maggi et al.*, 2000a, 2000b] that almost all the seismicity in deforming continents is in the crust, has prompted a reevaluation of the strength of the lithosphere, with the suggestion that it also lies mainly in the crust. In this view, the mantle must be wet and weak and unable to support significant elastic stresses [*Jackson*, 2002; *Maggi et al.*, 2000a, 2000b].

[5] The debate over the rheology of the lithosphere stems from the problems of untangling and directly measuring the in situ rheological properties of the crust or mantle. Understanding mantle behavior is particularly difficult because the mantle is largely hidden from view, at depths of several tens of kilometers. The only available samples tend to be nodules in volcanic rocks or deformed slivers preserved in mountain belts, and none of these may be representative of the bulk of the mantle at depth.

[6] One major structure that cuts through both the crustal and mantle parts of the lithosphere is the megathrust along the plate interface in a subduction zone (Figures 1 and 2). Thus the rheological properties of this fault zone could potentially place constraints on the rheology of both the crust and mantle, at least in this particular tectonic setting, as well as helping to determine the factors that control the strength of faults. Also, the resultant stresses will play a large role in determining both the rate and amount of deformation in the overriding plate, including the maximum elevations that can be supported, because the forces required must be transmitted across the plate interface [*Lamb and Davis*, 2003].

[7] It is striking that in subduction zones where the overriding plate is continental lithosphere, the maximum elevations in the deforming crust along or behind the volcanic arc are usually in the range 1−2.5 km (with trench-mountain relief 3.5−8 km), and the maximum crustal thickness is <45 km (Figures 1 and 3). This suggests that there is some general consistency in megathrust shear stresses from one subduction zone to another. However, the central Andes are a clear exception to this pattern. Here, maximum elevations in the overriding plate are between 4 and 5 km (with trench-mountain relief >11 km), and the crustal thickness exceeds 60 km (Figure 2). The large buoyancy force contrasts created by such large elevations and crustal thicknesses suggest that the average shear stresses on the subduction megathrust are substantially higher here than elsewhere [*Lamb and Davis*, 2003].

[8] So, what determines the shear stresses in subduction zones? Apart from the usual rheological parameters of pressure and temperature, there might be specific compositional effects, either in the crust or mantle, or variations in pore fluid pressure. Such compositional or pore fluid effects could be the result of the introduction of some specific "lubricant." Changes in any of these factors could have a significant effect not only on the total shear force, but also the tectonics of the deforming lithosphere itself, leading to a phase of intense shortening and uplift, if the shear force increases, or extension and collapse if it decreases. Thus knowledge of the mechanics of the subduction megathrust could improve our understanding of the geological evolution of the overriding plate.

[9] In this paper, these ideas are pursued by looking at the overall force balance in subduction zones, and in particular, shear stresses along the subduction megathrust. Analyzing these stresses in the context of the crustal and mantle structure, as well as temperatures and pressures, can help to constrain the rheological parameters at various depths in the lithosphere.

2. Forces and Stresses in a Subduction Zone

2.1. Estimating Subduction Megathrust Shear Stresses

[10] There have been a number of attempts to determine shear stresses (τ) on a megathrust by estimating its thermal structure from heat flow data [*Molnar and England*, 1990; *Tichelaar and Ruff*, 1993; *Peacock*, 1996]. *Molnar and England* [1990] showed that the thermal structure along the megathrust, for convergence at velocity V, depends principally on the heat flow from the subducted slab (Q_0), which is related to the age of the slab, and heat generation along the megathrust from shear heating (τV), ignoring any radiogenic heat production (likely to be small in subduction
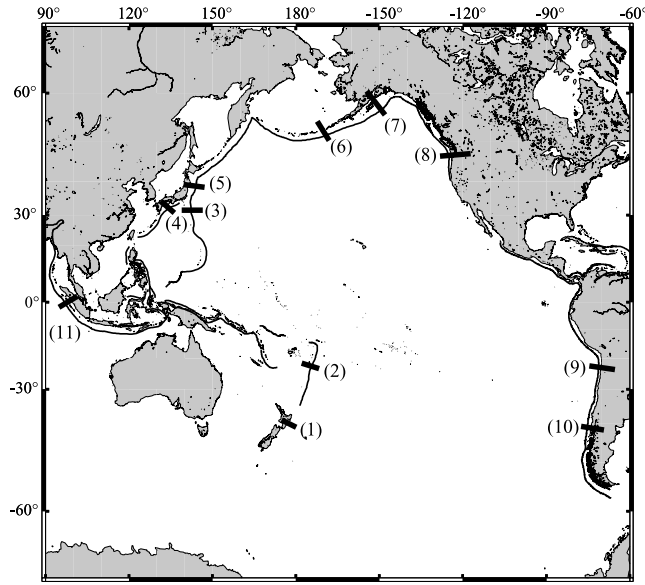
Figure 1. Subduction zones border most of the Pacific Ocean, and also the western margin of the Indian Ocean. Transects of subduction zones analyzed in this study are labeled 1 to 11 (see Table 1a).

settings; see section 3.3.2). The heat flow at the surface (Q) is only a small proportion of these heat sources, reduced by a factor S because of the subduction process itself, for a megathrust at depth z_f [*Molnar and England*, 1990; *Tichelaar and Ruff*, 1993]:

$$Q \approx \frac{(Q_0 + \tau V)}{S} \qquad (1)$$

where

$$S = 1 + b\frac{k'}{k}\sqrt{\frac{Vz_f^2}{y\kappa}}$$

and y is the distance along the length of the megathrust from the trench, κ is the thermal diffusivity, k and k' are the thermal conductivities in the overlying wedge and sub-

ducted slab, respectively, and b is a factor close to one. This way, heat generation from shear heating (τV), and hence the shear stresses themselves, can potentially be constrained from surface heat flow measurements. Unfortunately, heat flow measurements are generally sparse and prone to large uncertainties. In particular, it is unclear how much of the heat flow is by conduction or advection. In a subduction setting, where there is abundant evidence for fluid movement, advection may be important, resulting in a significant under or overestimate of the full heat flow. Nonetheless, heat flow studies, combined with full thermal modeling of particular subduction zones, have generally shown that we should anticipate megathrust shear stresses in the range 1–100 MPa, with mean shear stresses around 15 MPa [*Molnar and England*, 1990; *Tichelaar and Ruff*, 1993; *Hyndman and Wang*, 1993; *Peacock*, 1996]. These shear stresses are consistent with the PT conditions required for observed metamorphic reactions in subduction zones [*Peacock*, 1996].

[11] An alternative method is to estimate the shear stresses directly from the force balance in the deforming wedge above the megathrust [*Smith*, 1981; *Lamb and Davis*, 2003; *Hall*, 2003]. This is because the forces that drive deformation at a subducting plate boundary are transmitted across the plate interface, and therefore depend on the shear stresses along the megathrust. This work has yielded average shear stresses comparable to those determined from heat flow studies, but without many of the problems of the heat flow studies. In the following sections, the theory for this approach is developed more fully.

2.2. Subduction Zone Force Balance

[12] The widths of subduction zones are generally much less than the distances they extend along the trench. This low width to length ratio suggests that it is a good approximation to treat them as essentially two-dimensional structures, viewed in cross section. In this case, there must be a balance of all the forces in the plane of section. In particular, we can consider a roughly triangular wedge of lithosphere that overlies the subduction megathrust (Figure 4a). This wedge extends from the trench to where the megathrust cuts through the entire lithosphere. Thus the back of the wedge will be somewhere in the forearc, because the volcanic arc most likely overlies the corner flow in asthenospheric mantle, where long-lived mantle
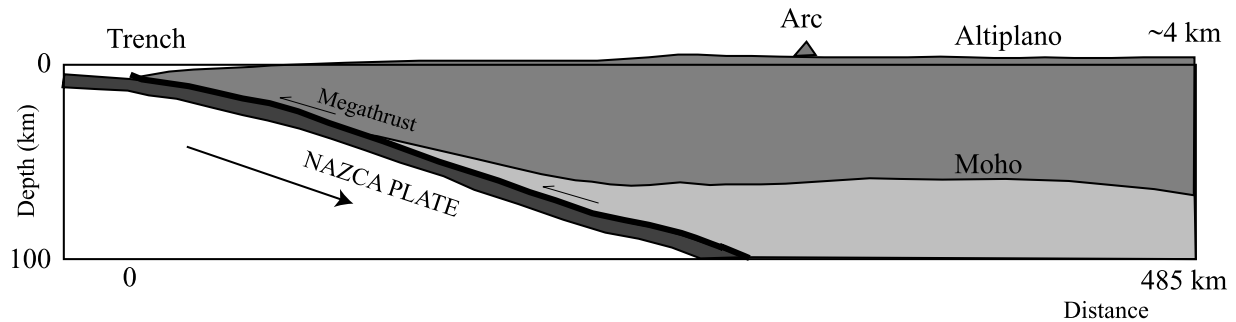

Figure 2. Lithospheric structure across the Peru-Chile subduction zone in northern Chile at ~21°S, based on seismic reflection and refraction studies [*Asch et al.*, 2003], clearly showing the megathrust at the plate interface as an inclined planar feature cutting through the lithosphere with a dip ~20°. The lithosphere above the megathrust forms an approximately triangular wedge.
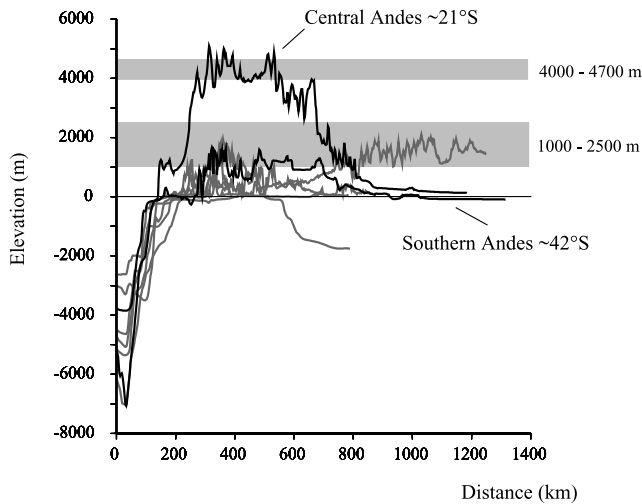
Figure 3. Bathymetric and topographic profiles of selected subduction zones analyzed in this study, where the volcanic arc is above sea level. See Figure 1 for location of transects. Trench depths are in the range 2.5 to 7 km below sea level, whereas the maximum elevations above sea level are almost all in the range 1 to 2.5 km. These give rise to maximum elevation contrasts between 3.5 and 8 km. The Peru-Chile subduction zone in northern Chile is a clear exception to this, having both the deepest trench ($\sim$7 km below sea level) and the highest elevations, reaching over 4 km above sea level, with an elevation contrast greater than 11 km.

melt generation is taking place. Ignoring tractions along the wedge surface, as well as inertial forces, leaves a simple balance of the forces on the remaining two sides (Figure 4b).

[13] For an idealized planar megathrust, the forces in cross section (per unit arc length) can be resolved into components parallel and perpendicular to the sides of the triangular wedge, and the shear force (F_s), or average shear stress (τ_s), parallel to the megathrust, can be expressed in terms of the body force within the wedge (Mg), and the components of push at the back of the wedge (P, and F_p or equivalent shear stress τ_p) (Figure 4b).

$$F_s + Mg\sin\theta + F_p\sin\theta = P\cos\theta \qquad (2)$$

where θ is the dip of the megathrust. Given that the lithosphere near a volcanic arc is likely to be hot and weak, with a relatively low flexural strength (elastic thickness Te $\ll$ 20 km), the principal stresses at the back of the wedge, close to the volcanic arc, are nearly horizontal and vertical, and F_p plays a relatively minor role. For lithosphere with a thickness L, $F_s \sim L\tau_s/\sin\theta$, $F_p \sim L\tau_p$, and $F_s \gg F_p\sin\theta$, and the force balance can be simplified by ignoring F_p, so (per unit arc length):

$$F_s \approx P\cos\theta - Mg\sin\theta \qquad (3)$$

The shear force along the megathrust is the difference between the push at the back of the wedge, and the weight of the wedge itself, both resolved parallel to the megathrust. For any given push, the lighter the wedge, the greater this shear

force will need to be. The shear force can be expressed in terms of the average shear stress (τ_s) on the megathrust. Therefore, if the wedge is a perfect triangle with a mean density ρ, and the height difference between the wedge tip and back is h, then equation (3) can be rewritten as

$$\tau_s \approx 0.5\left[\frac{P}{L} - \frac{\rho g(L-h)}{2}\right]\sin 2\theta \qquad (4)$$

where P/L is the mean horizontal normal stress at its back. The average shear stress on the basal megathrust will increase with both the dip of the megathrust (up to 45°) and the mean horizontal normal stress, and also the height difference between the wedge tip and back.

[14] Equations (3) and (4) suggest that if the geometry and density structure of the wedge are known, in particular, the depth of the Moho, as well as the push at the back of the wedge, then the average shear stress on the megathrust can be determined. It is worth noting that although the force system in the underlying subducted slab does not play an explicit role in this analysis, it is implicit in it. Thus the negative buoyancy of the subducted slab will determine the
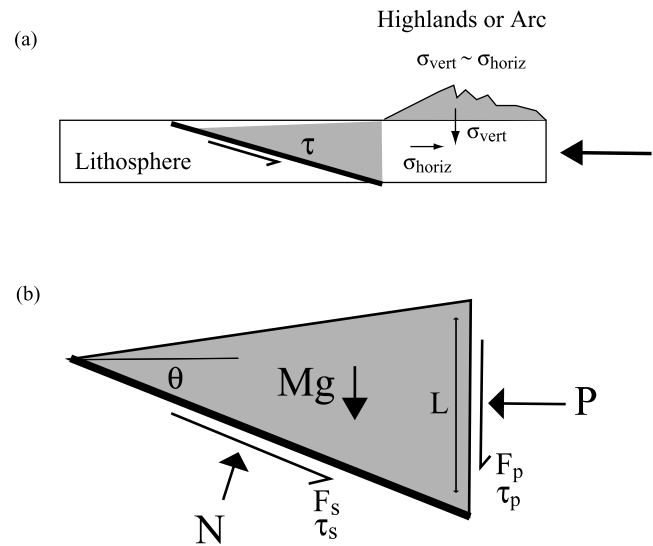

Figure 4. Diagrams illustrating the 2-D force balance in the plane of cross section through a subduction zone. (a) Megathrust cuts through lithosphere creating an overlying triangular wedge. The highlands or volcanic arc behind this wedge are often close to a state where the mean vertical normal stress balances the mean horizontal normal stress (i.e., there is no deviatoric stress in the plane of a trench- or arc-normal section). In this case, the elevation and crustal structure beneath the highlands can be used to determine the horizontal push that is transmitted across the subduction zone, balanced by the shear stress on the megathrust. (b) Definition of forces and stresses on lithosphere in the triangular wedge that overlies the megathrust, with dip θ. Without loss of generality, these forces and stresses can be resolved into components parallel (F_p, τ_p, F_s, τ_s) and perpendicular (P, N) to the sides of wedge (forces on the top surface of the wedge are negligible). In addition, there is an internal body force (Mg) caused by the weight of the wedge. See text.
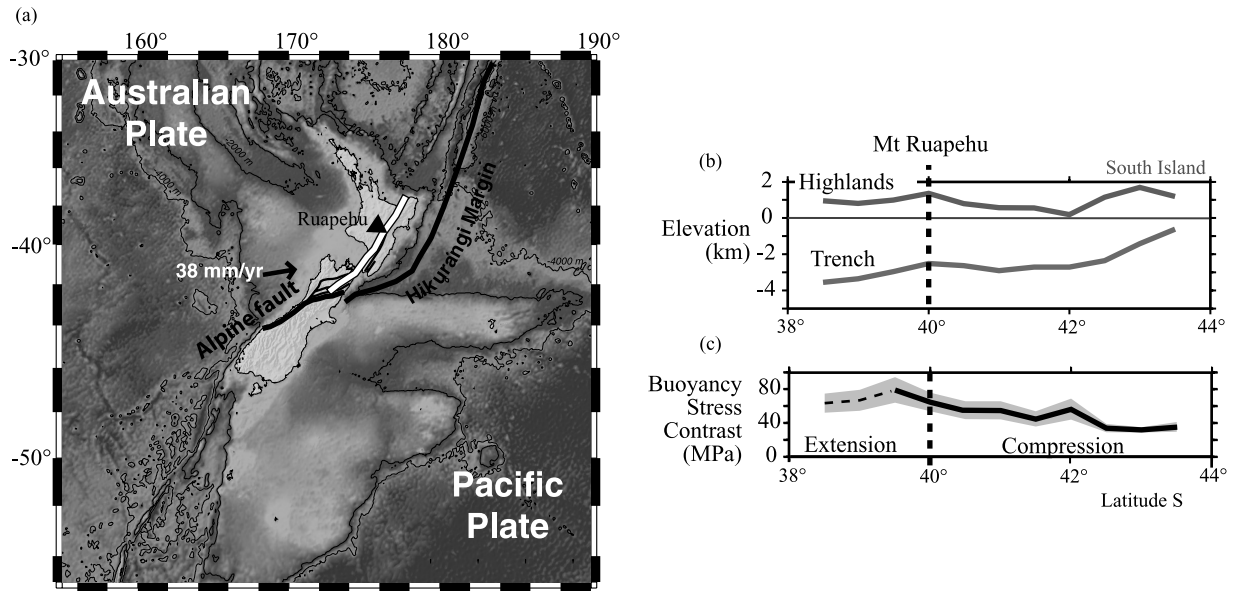
Figure 5. (a) Bathymetric map of the New Zealand region showing the location of the Hikurangi subduction zone, on the eastern side of North Island and the northern end of South Island. Black triangle shows the location of Ruapehu volcano, which marks the change over between back arc extension to the north, and compression to the south. Thick white line shows the line of the profiles illustrated in Figures 5b and 5c. (b) Diagram showing the variation in elevation of the highlands, and depth of the trench along the Hikurangi margin. (c) Diagram showing the variation in mean buoyancy stress contrast between the trench and highland, taken from *Hall* [2003]. The crossover at Ruapehu between behind arc extension and compression defines a reference buoyancy stress where deviatoric stresses in Hikurangi margin are close to zero. In this case, the deviation in buoyancy stress above or below this reference value, for the regions to the north and south, is generally <20 MPa, suggesting that deviatoric stresses here are <10 MPa.

amount of bending or curvature of the megathrust, and hence the depth of the trench, at the tip of the wedge, and also the magnitude of the vertical shear stress at the back of the wedge. However, as discussed above, the vertical shear stress at the back of the wedge only plays a very minor role in determining the average shear stress on the low-angle megathrust, and it is likely to be small anyway, because the back of the wedge, in the vicinity of the volcanic arc, is expected to be weak with a low flexural rigidity.

2.3. Constraining the Force at the Back of the Subduction Wedge

[15] The force P at the back of the wedge determines the deviatoric stresses in the lithosphere behind the wedge, in the highlands in the vicinity of the volcanic arc. For example, if there is no deviatoric stress beneath the highlands, in the plane of a vertical cross section normal to the arc or trench, then vertical normal stresses generated by the weight of rock beneath the highlands will balance horizontal normal stresses (Figure 4a), and P can be estimated by integrating the vertical normal stresses throughout the thickness of the lithosphere L [*England and Molnar*, 1997]:

$$P = g \int_0^L \int_0^z \rho(h)dhdz \qquad (5)$$

We can consider this case as defining the reference shear stress (τ_{ref}) on the megathrust. Thus, from equation (4),

allowing a deviatoric stress $\Delta\sigma$ (equivalent to adding or subtracting $2\Delta\sigma$ to P/L) will change the average shear stress on the megathrust by $\Delta\sigma\sin 2\theta$ ($\tau_s \sim \tau_{ref} \pm \Delta\sigma\sin \theta$). However, it is likely that the deviatoric stresses in the vicinity of the volcanic arc (in the plane of an arc-normal cross section) are relatively low, because here the heat flow is high and presumably the lithosphere is "hot" and weak. For example, the maximum sustainable deviatoric stress at the base of the seismogenic zone is

$$\Delta\sigma_{max} \approx \mu^*(1 - \lambda)\rho g z_{seis} \qquad (6)$$

where μ^* is the coefficient of friction on any fault, λ is the pore fluid pressure as a fraction of the lithostatic pressure, and z_{seis} is the thickness of the seismogenic zone. The mean deviatoric stress $\Delta\sigma_{mean}$ down to this depth is just $0.5\Delta\sigma_{max}$.

[16] If the arc is not actually undergoing shortening or extension, then the mean deviatoric stress for lithosphere of thickness L is reduced by the factor z_{seis}/L, because the elastic lid (with thickness z_{seis}) would be supporting *all* the deviatoric stresses throughout the lithosphere. For a typical seismogenic zone along the arc <15 km thick, 100 km thick lithosphere, $\mu^* \sim 0.5$, $\lambda > 0.4$ (hydrostatic pressure), then $\Delta\sigma \ll 10$ MPa. An alternative approach to calculating $\Delta\sigma$ is to use a bulk viscous model. Bulk lithospheric viscosities are generally estimated to be in the range $10^{21}–10^{22}$ Pa s [*England and Molnar*, 1997; *Bourne*, 1996; *Lamb*, 2000]. If shortening or extensional strain rates in the arc are less than a relatively high value of 10^{-15} s^{-1}, then, again, deviatoric
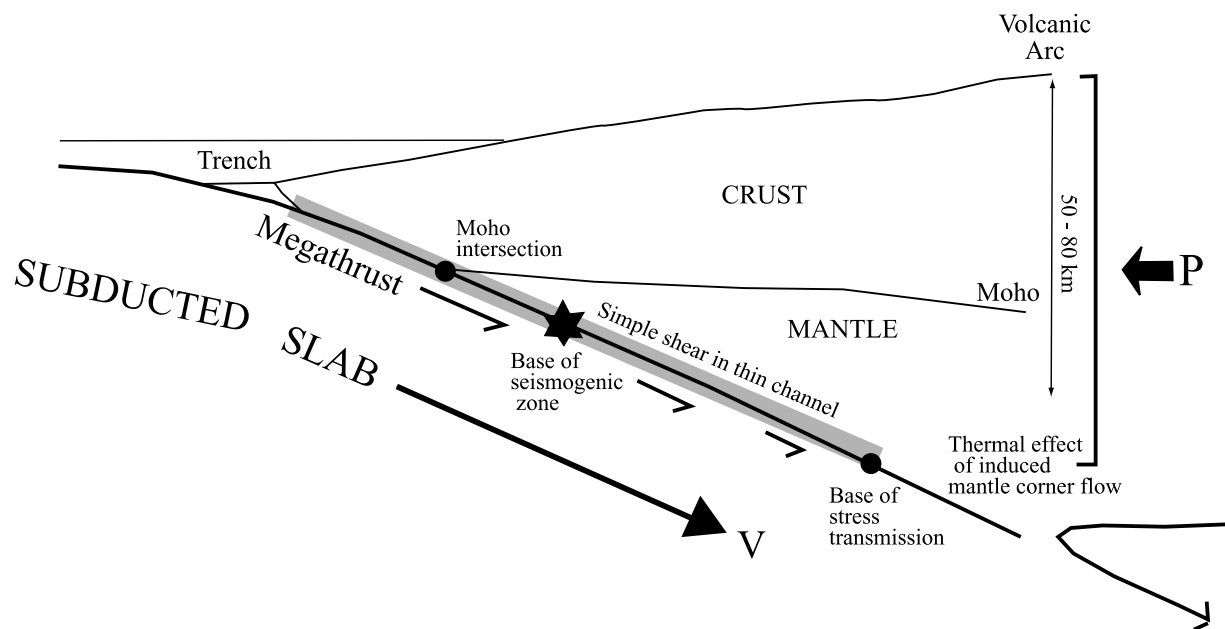
Figure 6. Diagram illustrating the main features of a megathrust in a subduction zone. In this study, it is assumed that almost all interplate slip is focused into a thin channel deforming by simple shear, accommodating subduction at velocity V. The base of the seismogenic zone defines the base of frictional slip on the megathrust, and the channel undergoes ductile flow at greater depth. In addition, the intersection of the Moho with the megathrust marks a change in the composition of the rocks in the upper plate, which may also be associated with a change in the rheology of the megathrust from that dominated by the properties of crustal rocks to one dominated by those of mantle rocks. Finally, the induced corner flow near the bottom of the lithosphere significantly raises the temperatures on the megathrust, defining the base of the zone of tress transmission. A push P, at the back of the overlying wedge, balances the forces in the subduction zone.

stresses will be less than 10 MPa. From equation (4), this translates into an additional average shear stress on the megathrust, for $\theta < 20°$, which is much less than 5 MPa. Thus, if volcanic arcs are shortening or extending at strain rates $<10^{-15}$ s^{-1}, then it should be possible to estimate from equations (4) and (5) the average shear stress on the plate interface to much better than 5 MPa, or $\ll 30\%$ if the mean shear stress is a typical value, suggested by heat flow studies, of ~ 15 MPa.

[17] More support for these conclusions comes from considering the force balance across the Hikurangi subduction zone in North Island, New Zealand [*Hall*, 2003] (Figure 5). Here, behind arc deformation changes along strike, from extension in the north to compression farther south. The change over from extension to compression takes place at the latitude of Ruapehu volcano (Figure 5b), at the southern tip of the Taupo Volcanic Zone. This region, then, is truly close to a state of balance between horizontal and vertical normal stresses, with essentially no deviatoric stress, and should provide a good estimate of the mean shear stress on the subduction megathrust. We can then calculate the deviatoric stresses in the behind arc region from the variation in buoyancy stress contrast, above or below the reference value, farther north and south, where the behind arc region is either in compression or extension (Figures 5b and 5c). This clearly shows that the deviatoric stresses driving deformation are $\ll 10$ MPa, in line with the conclusions of *Bourne* [1996] for the same region, based on a

consideration of viscous flow forces and buoyancy force contrasts in the deforming lithosphere.

[18] Finally, *Lamb and Davis* [2003] showed from the pattern of Quaternary tectonics in the high Andes, following the Peru-Chile subduction zone on the western margin of South America, that deformation flips over short distances between extension and compression or strike slip. This suggests, as in the Hikurangi margin, that deviatoric stresses, in the plane of a cross section normal to the arc, are very close to zero everywhere. Viscous modeling of the deformation, using a thin sheet continuum model of continental deformation, and given the low topographic gradients in the high Andes (defining the Altiplano plateau), also suggests negligible deviatoric stresses [*Husson and Ricard*, 2004].

[19] Very low deviatoric stresses (in the plane of a trench- or arc-normal cross section) beneath the highlands behind a subduction zone do not necessarily mean that there is no crustal deformation anywhere, only that any deformation is either strike-slip parallel to the trench, or is occurring at lower elevations.

3. Rheology and Temperatures Along the Megathrust

[20] In the previous analysis, only the average shear stress on the subduction megathrust has been considered. However, shear stresses might be expected to vary and be strong functions of pressure, temperature and composition. In
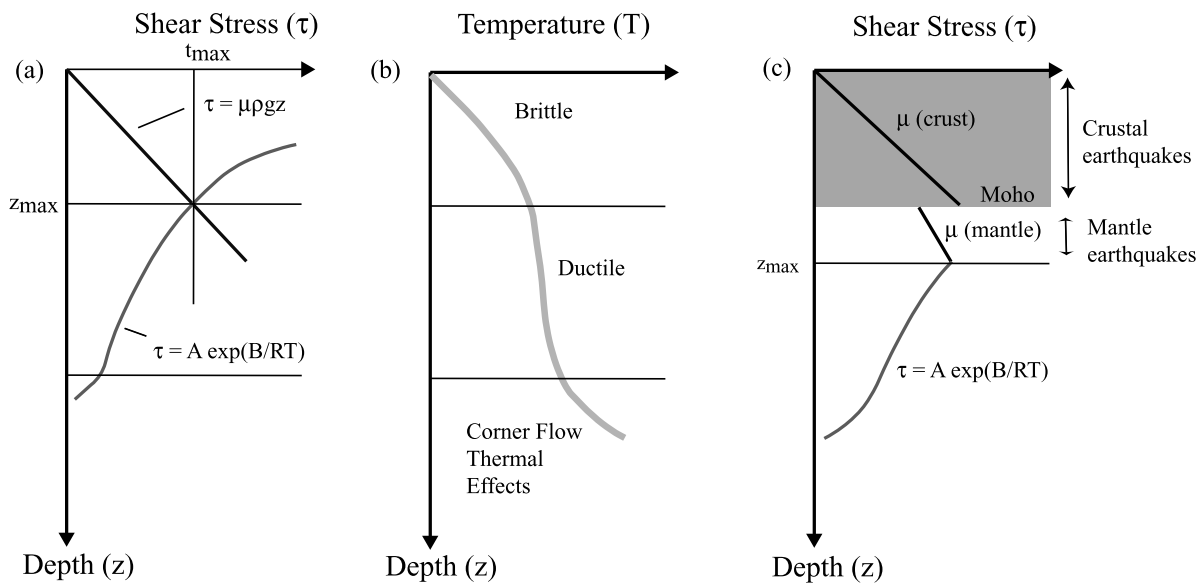
Figure 7. Plots illustrating the variation in shear stress (τ) and temperature (T) with depth (z) along the megathrust, assuming simple brittle and ductile rheologies. (a) Shear stress increases linearly with depth ($\tau = \mu\rho gz$) at shallow depths, where the megathrust is brittle, reaching a maximum value at the brittle-ductile transition. At greater depths, the stress required for brittle failure exceeds that for ductile flow, and the megathrust becomes a ductile shear zone. Here, shear stresses will be strongly controlled by temperature, following a Dorn-type exponential relationship ($\tau = A\exp(B/RT)$). (b) Temperature along the megathrust will be strongly influenced by shear heating (τV) and heat flow from the subducted slab. For the rheologies illustrated in Figure 7a, this will lead to an overall increase in temperature with depth, increasing more or less linearly in the brittle zone before flattening off in the ductile parts. Heat advection in the induced corner flow at depth will cause a marked increase in temperature at the bottom end of the megathrust. (c) Shear stress and temperature variations along the megathrust, illustrated in Figures 7a and 7b, are further complicated by the presence of a crust and mantle in the overlying wedge, with different rheological properties. This could lead to a marked jump in shear stress at the Moho, as well as the potential for a brittle-ductile transition in either the crust or mantle. The seismicity of the megathrust provides clues to the location of these brittle-ductile transitions.

principle, if one knew the rheology of the megathrust, in other words, the relation between shear stress and pressure, temperature, and composition, one should be able to calculate the shear stress distribution. In particular, it should be possible to assess the relative magnitudes of shear stresses where the megathrust cuts the crust and mantle of the overlying wedge.

[21] A simplified rheology of the brittle and ductile parts of the megathrust is outlined in the following sections. Although the rheology is probably more complex, the existence of a seismogenic zone at shallow depths, with essentially aseismic motion deeper down, suggests that this simplified approach describes the main features (Figure 6).

3.1. Brittle Deformation

[22] At shallow depths, in the seismogenic zone, where both pressures and temperatures are relatively low, the most plausible assumption is that the megathrust has frictional behavior (Figure 7). In this case, shear stresses would be expected to be proportional to normal stresses. For megathrusts with generally low dips, the normal stress is approximately the lithostatic pressure, and τ_s will follow equation (6), for a cohesionless fault:

$$\tau_s \approx \mu^*(1 - \lambda)\rho gz = \mu\rho gz \qquad (7)$$

where μ is now defined as the effective coefficient of friction, taking into account the pore fluid pressure. This behavior is assumed to extend down to some critical depth z_{crit}, determined by both temperature and pressure for any particular composition. Thus μ and z_{crit} will depend on whether the megathrust cuts the crust (μ_{crust}, $z_{crit(crust)}$) or mantle (μ_{mantle}, $z_{crit(mantle)}$) in the overlying wedge (Figure 7c).

[23] In the brittle domain, shear stresses are strongly pressure sensitive, but essentially independent of temperature.

3.2. Ductile Deformation

[24] Below the seismogenic zone, the megathrust might be expected to show plastic or viscous behavior, failing on timescales that are too long to generate earthquakes. In reality, this may be in parts frictional too, and there may be a broad transition to truly plastic/viscous behavior. However, following the usual definition of the brittle-ductile transition [*Ranalli*, 1995], this occurs where stresses required for some sort of crystal plastic deformation are smaller than those required for brittle failure. In this case, the brittle-ductile transition occurs where shear stresses on the megathrust are at a maximum (Figure 7a).

[25] In the ductile domain, experiments show that shear stresses show the converse relation to temperature and pressure expected in the brittle domain, and become strongly temperature (T) dependent. The relation that best describes the available experimental data is the Dorn equation [*Ranalli*, 1995], which can be reexpressed in very simplified form

$$\tau_s \approx A \exp\left(\frac{B}{RT}\right) \qquad (8)$$

where A and B are constants with units Pa and J mol^{-1}, respectively, and R is the universal gas constant and T is in kelvin. Strictly speaking, B will be a function of pressure too (but see below). Also, for viscous behavior, the factor A is a function of viscosity and strain rate (ε).

[26] It is likely that the megathrust is associated with an intense localized zone of deformation and strain weakening, which has operated for millions to tens of millions of years. In this case, ductile deformation is focused into a relatively narrow channel deforming by simple shear (Figure 6) [*Wdowinski and Bock*, 1994]. If the channel has a roughly constant width, then the strain rate across it will remain more or less the same along its length, and so A is effectively a constant for any particular megathrust; alternatively, A can be interpreted as some sort of average value. For simple shear, $\tau \propto \varepsilon^{1/n}$, where n is the power law exponent for flow (n = 1 for Newtonian viscous flow), and $A \propto \varepsilon^{1/n}$. Therefore, for large values of n, a constant A is an even better approximation: If n > 3, then for a channel width varying by up to a factor of 5, A will vary by less than a factor 1.7. For many types of plastic behavior, n might be expected to be even larger. In any case, the strain will tend to be focused into the weakest part of the channel.

[27] For a power law exponent n, the enthalpy for ductile flow is nB [*Ranalli*, 1995], where nB = E + PV, and E is the activation energy, P is the pressure, and V is the molar volume. For a typical subduction zone, we might expect ductile flow at the pressures for depths between 30 and 100 km. Taking typical values for E and V (V $\sim$ 10 $\times$ 10^{-6} m^3 mol^{-1}, E $\sim$ 150$-$500 kJ mol^{-1}), PV will be less than 10% of E, and to a very good approximation nB is constant and equal to E.

[28] The brittle-ductile transition in the crust or mantle is defined to occur at a depth z_{crit}, and temperature T_{crit}, where $\tau_{brittle} = \tau_{ductile}$ (Figure 7a):

$$\mu\rho g z_{crit} = A \exp\left(\frac{B}{RT_{crit}}\right) \qquad (9)$$

For $z < z_{crit}$, the megathrust is brittle, and for $z > z_{crit}$ it is ductile, and these conditions may apply independently to both the crust and mantle so that there may be brittle-ductile transitions in the crust and mantle (Figure 7c).

3.3. Megathrust Thermal Structure

[29] Determining the full thermal structure of a subduction zone is beyond the scope of this study. However, various authors [*Molnar and England*, 1990; *Tichelaar and Ruff*, 1993; *Peacock*, 1996; *England and Wilkins*, 2004] have shown that the steady state temperatures on

the subduction megathrust can be described to good approximation by simple analytical expressions. This is because the megathrust dips at moderate to low angles, and so the heat flow in the overlying wedge is predominantly vertical. Ignoring radiogenic heat production (see section 3.3.2), the steady state temperature gradients in the crustal or mantle parts of the overlying wedge are linear, and so the steady state temperature (T_f) on the megathrust, where it cuts the upper and middle parts of the lithosphere, follows the form of equation (1):

$$T_f \approx \frac{Qz_f}{k} = \frac{(Q_0 + \tau V)z_f}{kS} \qquad (10)$$

where k is the average thermal conductivity, z_f is the depth to the megathrust, and S is defined in equation (1). Note that the average thermal conductivity of the prism above the megathrust will depend on the crustal and mantle structure (see section A4) [*Tichelaar and Ruff*, 1993]. At greater depths, *Peacock* [1996] showed that the thermal effects of the corner flow in the asthenospheric wedge become important (Figures 6 and 7): Full thermal modeling suggests that this occurs at depths >50 km.

3.3.1. Mantle Corner Flow

[30] *England and Wilkins* [2004] present simple analytical expressions for the temperature at the top of the subducting slab where it forms a conductive boundary layer to the induced mantle corner flow. As with the shallower parts of the megathrust, these temperatures depend on the velocity of subduction, dip of the megathrust and age of the subducting slab (see section A5). Comparisons with full solutions [*Molnar and England*, 1990; *Peacock*, 1996; *England and Wilkins*, 2004] show that to good approximation, these expressions can be combined with equation (10) to determine the thermal structure along the whole length of the megathrust (section A5).

[31] It is clear from equations (8) and (10) that along the ductile portions of the megathrust, the temperature and shear stress are interrelated: Shear heating will influence the temperature, which in turn will determine, through the rheological relation, the amount of shear heating. Thus the temperatures will evolve to a steady state where the shear stress is sufficient to maintain both a constant temperature and shear stress.

[32] The importance of the corner flow to megathrust rheology is that it markedly raises the temperatures at the bottom end of the megathrust, with a drastic reduction (following equation (8)) in shear stress (Figures 7b and 7c). In effect, the thermal consequences of the corner flow determines the bottom termination of significant stress transmission across the plate interface (Figures 6, 7b, and 7c).

3.3.2. Radiogenic Heat Production

[33] Radiogenic heat production adds another heat source term for the temperature on the megathrust. If radiogenic heat production A is constant with depth, then the temperature effect at depth z_f on the megathrust (for $z_f \leq z_c$, where z_c is the local crustal thickness) is given by [*Tichelaar and Ruff*, 1993]

$$T_{rad} \approx \frac{Az_f^2}{2kS} \qquad (11)$$

Table 1a. Subduction Zone Parameters[a]

Label[b]	Subduction Zone	Latitude/ Longitude	Trench Depth (Fill),[c] km	Mean Dip	V,[d] mm/yr	Slab Age,[e] Ma	Heat Flow,[f] mW m^{-2}	Thrust Moho,[g] km	Max Depth,[h] km	Seismic Zone,[i] km	Maximum Height,[j] km
1	Hikurangi	40S/178E	3.5 (~2)	19°	36 ± 6	(120)	58 ± 10	34	81	40 ± 5	0.8 ± 0.2
2	Tonga	20S/174W	9.2 (<0.4)	24°	74 ± 6	120	44 ± 10	~10	78	40 ± 5	−2.0 ± 0.2
3	Izu-Ogasawara	32N/140E	9.8 (>0.4)	23°	51 ± 6	140	41 ± 10	~10	86	40 ± 5	−1.5 ± 0.2
4	Nankai	32N/134E	4.8 (~1.5)	12°	40 ± 6	15	124 ± 10	33	75	25 ± 5	1.0 ± 0.2
5	north Japan	39N/143E	7.6 (~1)	17°	88 ± 6	124	43 ± 10	20	81	40 ± 5	1.0 ± 0.2
6	Aleutian	51N/173W	7.0 (~2)	23°	65 ± 6	60	62 ± 10	10	78	40 ± 5	0.0 ± 0.2
7	west Alaska	60N/147W	5.1 (~2)	12°	56 ± 6	46	71 ± 10	33	85	33 ± 5	1.75 ± 0.2
8	Cascadia	46N/124W	2.6 (~2)	13°	44 ± 6	10	152 ± 10	35	87	25 ± 5	1.5 ± 0.2
9	north Chile	21S/70W	7.1 (<0.4)	20°	75 ± 6	(50)	40 ± 10	40	84	45 ± 5	4.0 ± 0.2
10	south Chile	42S/72W	3.8 (~2)	20°	70 ± 6	17	116 ± 10	43	82	43 ± 5	1.4 ± 0.2
11	Sumatra	0/99E	5.4 (>1)	24°	40 ± 6	(50)	70 ± 10	33	79	45 ± 5	1.5 ± 0.2

[a]With 2σ uncertainties.

[b]See Figure 1; profiles are from (1) *Stern and Davey* [1989], (2) *National Earthquake Information Center (NEIC)* [2003], (3) *Suyehiro et al.* [1996], (4) *Kodaira et al.* [2000], (5) *Takahashi et al.* [2004], (6) *Holbrook et al.* [1999], (7) *Moore et al.* [1991], (8) *Parsons et al.* [1998], (9) *Asch et al.* [2003], (10) *NEIC* [2003], and (11) *Simones et al.* [2004].

[c]Depth of trench axis, with thickness of axial sedimentary fill in brackets [*von Huene and Scholl*, 1991].

[d]Component of trench normal slip velocity on megathrust (NUVEL-1A [*DeMets et al.*, 1994; *England et al.*, 2004; *Angermann et al.*, 1999]).

[e]Ages in parentheses not used to calculate heat flow [*Muller et al.*, 1997].

[f]Heat flow from top of subducted slab, calculated from $480/age(Ma)^{0.5}$ relation after *Parsons and Sclater* [1977].

[g]Depth of intersection of Moho in overlying wedge with megathrust.

[h]Maximum depth extent of megathrust considered in this study.

[i]Maximum depth of interplate slip earthquakes.

[j]Maximum elevation in arc or behind arc region.

where k is the thermal conductivity and S is the subduction advection factor, defined in equation (1).

[34] Estimates for radiogenic heat production in accretionary prisms are generally in the range 0.4–1.0 μW m^{-3} [*Hyndman and Wang*, 1993; *Springer*, 1999; *Simones et al.*, 2004], applied to the whole thickness of the crust. In this case, radiogenic heating adds an extra heat source term ≪18 mW m^{-2} for crust ≤35 km. These values can be compared with the heat flow from the subducted plate, which is in the range 40 to 150 mW m^{-2}, and heat flow from shear heating which is in the range 25–70 mW m^{-2} (for a shear stress of ~25 MPa at depths ~30 km). Thus radiogenic heat production in the crust accounts for ≪20% of total heat flow, and its effect (T_{rad}) is to raise the megathrust temperature generally by not more than 30°C.

4. Determining Megathrust Rheological Constants

[35] The shear stresses and thermal structure of the megathrust must be solved for simultaneously, using equations (8), (10) and (11), and this requires knowledge of the rheological constants (A, B, μ). However, there are some important constraints because both the average or integrated shear stress (total shear force from the force balance, equation (3)) and pressures along the megathrust are taken as known. Unfortunately, these constraints are insufficient to calculate the constants. Indeed, assuming that the rheological constants are different for crust and mantle, even in this simplified analysis there are 6 unknowns in all, while a knowledge of the average or integrated shear stress provides only one constraint. The situation can be improved by assuming that the maximum depth of plate interface slip earthquakes marks the brittle-ductile transition (in crust or mantle), adding an additional constraint (i.e., $z_{crit} = z_{seis}$ in equation (9)).

[36] One way of making progress is to examine whether the rheological constants for the crust and mantle are common to several subduction zones. Given enough subduction zones, a solution can be found for the constants by considering the force balance and thermal structure in each one, using standard inverse theory [*Menke*, 1988] in an overdetermined problem (see section A1).

4.1. Subduction Zones

[37] In this study, eleven subduction zones are analyzed (Figure 1 and Table 1a). These have been selected mainly on the basis of the availability of detailed data on the crustal structure, geometry and seismicity, derived from seismic refraction, reflection or gravity studies. For example, high-resolution refraction and reflection studies across the Andean subduction zone at 21°S [*Asch et al.*, 2003], or Cascadia [*Parsons et al.*, 1998] in western North America, or northeastern and western Japan [*Kodaira et al.*, 2000; *Takahashi et al.*, 2004], or the eastern Aleutians [*Holbrook et al.*, 1999], have revealed the detailed velocity structure, constraining not only the slab and Moho geometry, but also the crustal and mantle densities. The bathymetry and topography are taken from the *GEBCO* [2003] data set.

[38] The selected subduction zones have the added advantage that there is considerable variability in rate of convergence (36–88 mm/yr), age of the subducted plate (10–140 Ma), crustal thickness at the Moho intersection with the megathrust (<10–40 km), composition of the crust (mafic to felsic), and the presence of potential lubricants such as trench sediment fill (trench axis sediment fill from <0.4 to >2 km). Thus a study of these subduction zones has the potential to explore the full range of factors that might control shear stresses along the megathrust. The essential features are listed in Tables 1a and 1b.

4.2. Inversion Methodology

[39] Full details of the inversion method are given in section A1. It is desirable when inverting for the rheological constants to make the problem as overdetermined as possible, so that the number of constraints should greatly exceed

Table 1b. Inversion Parameters[a]

Parameter	Value
Crust reference density	2800 kg m^{-3}
Mantle reference density	3300 kg m^{-3}
Prism crust density contrast	-90 ± 50 kg m^{-3}
Prism mantle density contrast	-50 ± 30 kg m^{-3}
Corner flow depth	65 ± 15 km
Slab thermal conductivity	2.9 W m^{-1} °C^{-1}
Crust thermal conductivity	2.5 W m^{-1} °C^{-1}
Mantle thermal conductivity	3.3 W m^{-1} °C^{-1}
Thermal diffusivity	10^{-6} m^2 s^{-1}
Mantle reference temperature	1280°C
Constant crustal radiogenic heat production	0.65 ± 0.3 μW m^{-3}

[a]With 2σ uncertainties.

the number of constants that need to be determined. In principle, given enough subduction zones, assuming that any particular set of constants is common to them all, it should be possible to solve for all 6 constants defined in equations (7) and (8) (μ_{crust}, μ_{mantle}, A_{crust}, A_{mantle}, B_{crust}, B_{mantle}). In reality, because the seismogenic zone for almost all the subduction zones considered extends at least to the base of the crust, the inversion procedure has limited resolving power for the ductile behavior of the crust, but places substantial constraints on its frictional behavior. However, both the frictional and ductile behavior of the mantle should be resolved. Bearing all this in mind, it is sufficient to simplify the problem by setting B_{crust} to be equal to B_{mantle}.

[40] The A constants can be determined for each subduction zone individually, given by the constraint that the base of the seismogenic zone coincides with the brittle-ductile transition, as defined in equation (9). However, because the subduction zones all appear to have only one brittle-ductile transition, which is usually, as remarked on above, either close to the base of the crust or in the mantle, there is some uncertainty about the rheology of the individual potential crust or mantle brittle-ductile transitions. Again, I simplify the problem by assigning them to be the same. This is likely to be a good approximation, because if the actual observed brittle-ductile transition is in the mantle, then the potential crustal one must be deeper than the actual depth of the crust. Likewise, if it is in the crust, then the potential mantle one must be shallower than the depth of the crust. Given the uncertainties in determining the base of the seismogenic zone (±5 km), this simplification is within the data uncertainties we are dealing with (see below).

[41] Monte Carlo simulations (see section A1) were carried out by perturbing all input data within likely error bounds, assuming a normal distribution for these uncertainties. There is a strong trade off between A and B, and a small change in B, because it appears as an exponential power, can have a large effect on A. However, it is important to realize that whatever A and B turn out to be, the magnitudes of the shear stress (combined effect of A and B in equation (8)) are well constrained because they are set by the overall force balance constraint. However, in cases where the slip vector on the megathrust is not normal to the trench, an adjustment is needed to the force balance and thermal equations (see section A7).

[42] The following sections describe the results of experiments in which the rheological constants are solved using

different combinations of subduction zones (see Tables 2−5). In each subduction zone, a solution for five constants is sought: μ_{crust}, A_{crust}, μ_{mantle}, A_{mantle}, B. A_{crust} and A_{mantle} are solved individually for each subduction zone, using equation (9), and may be properties of the convergence rate and local megathrust geometry. This leaves 3 constants (μ_{crust}, μ_{mantle}, B) that are of general significance for a range of subduction zones. The degrees of freedom (DF) in any inversion is approximately N − n, where N is the number of subduction zones used and n is the number of unknowns minus constraints (Table 2). An informal measure of the goodness of fit is F_{min}/DF, where F is the function that we seek to minimize (equation (A1)). The fit can also be estimated by determining the mean misfit in MPa between the average shear stress on the megathrust determined from the rheology and from the force balance.

5. Results

[43] The following experiments are based on three different groupings of the subduction zones in Figure 1 and Table 1a. All uncertainties are quoted at the 1σ level unless otherwise indicated. The values of various input parameters used in the inversions are shown in Tables 1a and 1b, and the results are shown in Tables 2−5. An important input parameter is the depth at which the thermal structure of the megathrust starts to be dominated by the effect of the corner flow. In the experiments, it is constrained to lie anywhere in the plausible range 50 to 80 km (65 ± 15 (2σ)). Radiogenic heat production is taken as constant throughout the crust, in the range 0.4−1.0 μW m^{-3} (0.65 ± 0.3 μW m^{-3} (2σ)).

5.1. Experiment 1 (Table 3)

[44] In this experiment, a solution for the rheological constants was sought that was common to all 11 subduction zones. The global minimum for F (equation (A1)) is 2792×10^{22} N^2 m^{-2}, with a goodness of fit (F_{min}/DF) equaling 349×10^{22} N^2 m^{-2} and a mean shear stress misfit of ∼4.1 MPa, or ∼28% of the mean average shear stress. The effective coefficients of friction in the crust and mantle are 0.031 ± 0.006 and 0.027 ± 0.004, respectively, and B is 37.05 ± 18.13 kJ mol^{-1}.

[45] It is clear that one subduction zone, northern Chile, contributes most of the misfit. The maximum elevations here are markedly greater, by a factor of 2 or more, than those for all the other subduction zones. However, the larger shear force or average shear stress on the megathrust needed to balance this requires a different rheology here and cannot be explained solely in terms of the subduction parameters such as the geometry of megathrust, age of subducted plate, or crustal structure within the wedge.

5.2. Experiment 2 (Table 4)

[46] Experiment 2 repeats experiment 1, but this time northern Chile is excluded from the set of subduction zones (Table 4). There is a marked improved in the fit (compare with experiment 1), and now the global minimum for F (equation (A1)) is over 3 times less at 819×10^{22} N^2 m^{-2}, with a goodness of fit (F_{min}/DF) equaling 117×10^{22} N^2 m^{-2} and a mean shear stress misfit of ∼2.9 MPa, or about 26% of the mean average shear stress. There is essentially no difference in the effective coefficient of friction for the

Table 2. Inversion Results for Experiments 1–3

Experiment	N (n)[a]	DF[b] (N − n)	F[c] 10^{22} N² m⁻²	F/DF, 10^{22} N² m⁻²	μ_c[d]	P_f^e %	μ_m[d]	P_f^e %	B, kJ mol⁻¹	μ_c'[d]	P_f^e %	μ_m'[d]	P_f^e %
1	11 (3)	8	2792	349	0.031 ± 0.006	94	0.027 ± 0.004	95	37.05 ± 18.13				
2	10 (3)	7	819	117	0.028 ± 0.006	94	0.020 ± 0.004	96	32.62 ± 23.16				
3	11 (5)	6	631	105	0.032 ± 0.005	94	0.019 ± 0.004	96	36.32 ± 18.06	0.095 ± 0.024	81	0.026 ± 0.007	95

[a]N, number of subduction zones analyzed; n, number of common rheological parameters solved for.
[b]Degrees of freedom, N minus n.
[c]Least squares fit F(μ, A, B); see equation (A1).
[d]The parameters μ_c and μ_m, the effective coefficients of friction for the crust and mantle, respectively, in all subduction zones analyzed, except in experiment 3 where μ_c' and μ_m' are those for subduction zones 2 and 9.
[e]Pore fluid pressure as a fraction (λ) of lithostatic pressure (see equation (7)), assuming a typical frictional sliding coefficient of 0.5.

crust, compared to that in experiment 1, at 0.028 ± 0.006, though there is a slight reduction in this for the mantle (0.020 ± 0.004), and B is less at 32.62 ± 23.16 kJ mol⁻¹.

[47] It is clear from Table 1a that the only feature that clearly distinguishes the subduction zone in northern Chile from all the others, except Tonga, is the lack of significant (<0.4 km) axial trench fill. This observation prompted *Lamb and Davis* [2003] to suggest that subducted trench sediments act as a lubricant along the plate interface, because they smooth it out and allow water to be carried to greater depths, raising the average pore fluid pressure.

[48] Tonga, which also has essentially no trench fill, can be fitted together with the other subduction, zones. This could be easily explained if any potential lubricating effect from trench sediments is mainly confined to the crust, and the crustal thickness in the Tonga subduction zone is small, around 10 km thick. These ideas can be tested by allowing the frictional constants for northern Chile and Tonga to be the same and independent of those for the other subduction zones.

5.3. Experiment 3 (Table 5)

[49] Both northern Chile and Tonga are excluded from the main set of subduction zones, and their frictional constants are solved for independently; this is close to an evenly determined problem, with two unknowns (μ_{crust} and μ_{mantle}) and the constraints given by the geometry and thermal structure of two subduction zones. The rheological constants for the other 9 subduction zones are markedly overconstrained (overdetermined problem). The existence of serpentinite diapirs in the trench above the Izu-Ogasawara megathrust [*Suyehiro et al.*, 1996] suggests that a mantle rheology is appropriate here for the crustal part of the megathrust as well. In any case, the significant thickness of both seafloor pelagic sediment and trench fill together (>0.4 km) suggests that this is a lubricated system.

[50] The results for subduction zones except northern Chile and Tonga are very similar to experiment 2. Thus the global minimum for F (equation (A1)) is 631 × 10^{22} N² m⁻², with a goodness of fit (F$_{min}$/DF) equaling 105 × 10^{22} N² m⁻² and a mean shear stress misfit of ~2.3 MPa, or about 21% of the mean average shear stress. B is 36.32 ± 18.06 kJ mol⁻¹.

[51] The effective coefficients of friction in the crust and mantle for northern Chile and Tonga are substantially higher (0.095 ± 0.024 and 0.026 ± 0.007, respectively), compared to the remaining subduction zones (0.032 ± 0.005 and 0.019 ± 0.004, respectively).

6. Discussion

[52] The good fits in experiments 2 and 3, and to a lesser extent, experiment 1, are remarkable because they show that shear stresses in such a wide range of subduction zones can be explained in terms of relatively few constants. For subduction zones except northern Chile and Tonga, average shear stresses are ≤15 MPa, despite huge variations in the age of the subducted plate and plate convergence rate; recalling section 2.3, even if there are deviatoric stresses in the highlands behind subduction zones, these would only change this value by <5 MPa. These low average shear stresses are consistent with those deduced from modeling of

Table 3. Experiment 1 Mean Solutions[a]

Subduction Zone	P_{obs}, 10^9 N m^{-1}	P_{calc}, 10^9 N m^{-1}	ΔP,[b] 10^9 N m^{-1}	τ_{diff},[c] MPa	τ_{mean},[d] MPa	P',[e] 10^9 N m^{-1}	T_{max}, °C Crust[f]	T_{max}, °C Mantle[f]	T_{bd}, °C Crust[g]	T_{bd}, °C Mantle[g]	A_{crust},[h] kPa	A_{mantle},[h] kPa
Hikurangi	96925	97776	851	3.3	13.2	3968	268	359	>268	316	19.3	8.6
Tonga	90041	89455	−586	−3.1	15.6	3351	70	477	>70	221	4.3	3.6
Izu	117482	119020	1538	6.8	13.2	3845	78	541	>78	211	3.6	2.5
Nankai	81529	82371	843	2.3	10.3	3802	495	605	454	<497	45.8	27.7
North Japan	96222	98283	2061	7.5	16.3	4793	140	493	>140	274	5.0	8.7
Aleutian	88858	88897	40	0.2	15.6	3488	94	424	>94	247	3.2	5.9
West Alaska	107246	107693	448	1.1	12.1	5344	372	406	365	<366	22.6	13.1
Cascadia	110940	109810	−1130	−2.8	7.2	2952	568	753	508	<553	68.9	18.2
North Chile	108883	104970	−3913	−15.5	21.8	5755	231	354	>231	276	4.4	10.9
Southern Chile	99682	100055	373	1.6	15.4	3689	468	508	>458	<401	127.4	17.3
Sumatra	91712	91453	−259	−1.3	18.9	4345	255	343	>255	326	27.5	17.1

[a]Constant crustal radiogenic heating = 0.65 ± 0.3 μW m^{-2} (2σ); corner flow at 65 ± 15 km (2σ). Mean rheological constants: μ_c = 0.031, μ_m = 0.027, B = 37.05.
[b]Difference between calculated and observed horizontal force P at back of subduction zone.
[c]Difference between calculated and observed mean shear stress on megathrust.
[d]Mean shear stress on megathrust.
[e]Total horizontal shear force on megathrust.
[f]Maximum temperature on megathrust in crust or mantle.
[g]Temperature of brittle-ductile transition in crust or mantle.
[h]Preexponential A constant in ductile rheology (see equation (8)).

surface heat flow measurements [*Peacock*, 1996] and also South American intraplate stress analyses [*Richardson and Coblenz*, 1994]. In the following discussion, experiment 3, which has the least misfit with the data, is the preferred solution (Figures 8–11).

[53] The thermal structure of the megathrusts (Figures 8–11) clearly has the major features described by *Peacock* [1996] and summarized in Figure 12. Thus temperatures increase more or less linearly down to the Moho, at depths of a few tens of kilometers (Figure 12a). Thereafter, the temperature profile flattens out until the thermal effects of the corner flow become dominant, and temperatures increase abruptly. The apparent discontinuity in temperature at the Moho is a consequence of the simple one-dimensional (1-D) approximation used here. This is particularly marked on the megathrust in northern Chile (Figure 11a), where the high shear stresses in the crustal part have resulted in much higher temperatures near the Moho intersection, compared to those in the underlying mantle. In reality, such a discontinuity would be more smoothed out by lateral heat flow. However, because the megathrust dips at shallow to moderate angles (<20°), vertical heat flow will still dominate, giving rise to a pronounced kink in the thermal profile (see section A6).

[54] The variation in shear stress down the length of the megathrust generally has a broad hump profile (Figure 12b), with a linear increase down to the brittle-ductile transition at depths of a few tens of kilometers, and then a broad region of more nearly constant shear stress, which markedly drops off at depths ≤80 km where the temperatures are strongly affected by the corner flow (Figure 12b). Exceptions to this general pattern are the hot Nankai and Cascadia subduction zones (Figures 8 and 10). Here, the megathrust brittle-ductile transition occurs at shallower depths than the Moho intersection, and shear stresses tail off below this.

Table 4. Experiment 2 Mean Solutions[a]

Subduction Zone	P_{obs}, 10^9 N m^{-1}	P_{calc}, 10^9 N m^{-1}	ΔP,[b] 10^9 N m^{-1}	τ_{diff},[c] MPa	τ_{mean},[d] MPa	P',[e] 10^9 N m^{-1}	T_{max}, °C Crust[f]	T_{max}, °C Mantle[f]	T_{bd}, °C Crust[g]	T_{bd}, °C Mantle[g]	A_{crust},[h] kPa	A_{mantle},[h] kPa
Hikurangi	96925	96998	72	0.3	10.7	3190	264	359	>264	292	40.3	12.4
Tonga	90041	88628	−1413	−7.4	11.8	2524	69	477	>69	189	10.1	4.5
Izu	117482	118094	613	2.7	10.1	2919	76	540	>76	184	8.6	3.5
Nankai	81529	81924	395	1.1	9.1	3354	492	601	450	<486	85.5	39.8
North Japan	96222	97135	913	3.3	12.5	3645	136	493	>136	232	11.2	9.5
Aleutian	88858	88013	−844	−4.2	11.6	2604	93	424	>93	221	8.0	8.0
West Alaska	107246	106887	−358	−0.8	10.3	4538	365	406	357	<341	44.8	17.8
Cascadia	110940	109554	−1386	−3.5	6.6	2695	566	753	504	<548	122.7	27.5
Southern Chile	99682	99544	−138	−0.6	13.3	3178	457	508	>457	<379	214.2	23.3
Sumatra	91712	90543	−1169	−5.9	15.1	3436	251	338	>251	300	55.6	23.1

[a]Constant crustal radiogenic heating = 0.65 ± 0.3 μW m^{-2} (2σ); corner flow at 65 ± 15 km (2σ)). Mean rheological constants: μ_c = 0.028, μ_m = 0.020, B = 32.62.
[b]Difference between calculated and observed horizontal force P at back of subduction zone.
[c]Difference between calculated and observed mean shear stress on megathrust.
[d]Mean shear stress on megathrust.
[e]Total horizontal shear force on megathrust.
[f]Maximum temperature on megathrust in crust or mantle.
[g]Temperature of brittle-ductile transition in crust or mantle.
[h]Preexponential A constant in ductile rheology (see equation (8)).

Table 5. Experiment 3 Mean Solutions[a]

Subduction Zone	P_{obs}, 10^9 N m^{-1}	P_{calc}, 10^9 N m^{-1}	ΔP,[b] 10^9 N m^{-1}	τ_{diff},[c] MPa	τ_{mean},[d] MPa	P',[e] 10^9 N m^{-1}	T_{max}, °C		T_{bd}, °C		A_{crust},[h] kPa	A_{mantle},[h] kPa
							Crust[f]	Mantle[f]	Crust[g]	Mantle[g]		
Low Stress Subduction Zones (μ_c = 0.032, μ_m = 0.019, B = 36.32)												
Hikurangi	96925	97051	125	0.5	11.0	3243	272	359	>272	288	25.2	4.6
Izu	117482	117785	303	1.3	8.9	2609	71	541	>71	179	1.2	1.1
Nankai	81529	82133	604	1.7	9.7	3563	498	598	457	<483	56.2	18.7
North Japan	96222	97047	825	3.0	12.2	3557	143	493	>143	224	7.0	3.2
Aleutian	88858	87851	−1006	−5.0	11.0	2442	95	424	>95	216	4.4	2.8
West Alaska	107246	107141	−105	−0.2	10.9	4792	379	406	371	<336	29.2	7.2
Cascadia	110940	109755	−1185	−3.0	7.1	2897	572	751	512	<545	83.5	12.8
Southern Chile	99682	99755	73	0.3	14.2	3389	478	508	>478	<373	161.9	9.7
Sumatra	91712	90550	−1162	−5.9	15.2	3442	258	338	>258	295	35.8	9.1
High Stress Subduction Zones (μ_c = 0.095, μ_m = 0.026, B = 36.32)												
Tonga	90041	89951	−90	−0.5	18.3	3847	113	477	>113	217	346.9	3.8
North Chile	108883	108895	12	0.0	36.7	9680	493	354	>493	270	317.9	11.3

[a]Constant crustal radiogenic heating = 0.65 ± 0.3 μW m^{-2} (2σ); corner flow at 65 ± 15 km (2σ).
[b]Difference between calculated and observed horizontal force P at back of subduction zone.
[c]Difference between calculated and observed mean shear stress on megathrust.
[d]Mean shear stress on megathrust.
[e]Total horizontal shear force on megathrust.
[f]Maximum temperature on megathrust in crust or mantle.
[g]Temperature of brittle-ductile transition in crust or mantle.
[h]Preexponential A constant in ductile rheology (see equation (8)).

6.1. Coefficients of Friction

[55] The effective crustal and mantle coefficients of friction on most megathrusts are similar and low. These low effective coefficients of friction, given a typical frictional sliding coefficient of ∼0.5 for clays [*Cartwright and Lonergan*, 1996], imply (using equation (7)) average pore fluid pressures ∼95% of lithostatic pressure. The effective coefficients are essentially the same as those determined from critical wedge theory for accretionary prisms, which are around 0.03 [*Lallemand et al.*, 1994]. *Lallemand et al.* [1994] estimate an average pore fluid pressure in subduction zones of ∼88% lithostatic pressure, which would suggest that the frictional sliding coefficient is ∼0.25, and nearer to the lower values for clays [*Bishop et al.*, 1971].

[56] The large shear force for the subduction zone in northern Chile requires an effective crustal coefficient of friction which is roughly 3 times greater than that for the low stress subduction zones. This could be explained simply in terms of a lower pore fluid pressure in the crust (∼81% lithostatic pressure) compared to elsewhere. Alternatively, it might reflect some compositional variation in the fault zone. In either case, these changes may be due to the absence of a specific lubricant, such as subducted trench sediments (see section 6.4). However, the effective mantle coefficient of friction (∼0.026) for northern Chile is the same within error to that for the other subduction zones, suggesting that any frictional lubrication effect is mainly confined to the crustal portion of the megathrust (see below).

6.2. Brittle-Ductile Transition

[57] The definition of the brittle-ductile transition used in this study (defined by equation (9)) is a function of both temperature and pressure and we should not expect it to occur at a unique temperature. In reality, the brittle-ductile transition is unlikely to be a simple rheological transition, but may be the result of a range of microstructural processes. Nonetheless, it is striking that in the crust it occurs at temperatures in the range ∼370°C to ∼515°C, very much

in line with experimental results [*Ranalli*, 1995]. However, the brittle-ductile transition seems to take place in the mantle at temperatures in the range ∼180°C to ∼300°C, though all these values are probably subject to an uncertainty of ∼10%, just from the uncertainty in the thermal conductivity. Thus it is clear that the temperature of the brittle-ductile transition in the mantle is lower than that for the crust. This may merely reflect the different properties of crustal and mantle materials, such as wet sediment, sheared granite or serpentinite, or could be because the transition in the mantle has a different physical basis, such as a marked change in pore fluid pressure or quasi ductile and subfrictional properties [*Simones et al.*, 2004].

[58] One intriguing implication of the variations in shear stress along the megathrust is that the stress peaks could be potential asperities or nucleation points for great earthquakes. For example, there is often a marked jump in shear stress at the crust-mantle boundary. Also, when the brittle-ductile transition is well within the mantle, there is an additional shear stress peak, creating a second possible earthquake nucleation point (see Figures 9, 10, northern Japan and Sumatra).

6.3. Ductile Flow

[59] The inversions require the ductile part of the megathrust in many subduction zones to contribute a substantial proportion of the total shear force (section 6.5). From the point of view of the thermal structure of the megathrust, a subduction zone is an extraordinarily buffered large-scale dynamic system. Thus increasing plate convergence has two competing effects, raising temperatures through increased shear heating, but decreasing them too through increased downward advection. Cooling of the ductile part of the megathrust will increase shear stresses, which will result in heating from increased shear heating. Thus, for the range of conditions on the earth, almost all subduction zones seem incapable of sustaining shear stresses along the megathrust that would be able to support elevations in the overriding
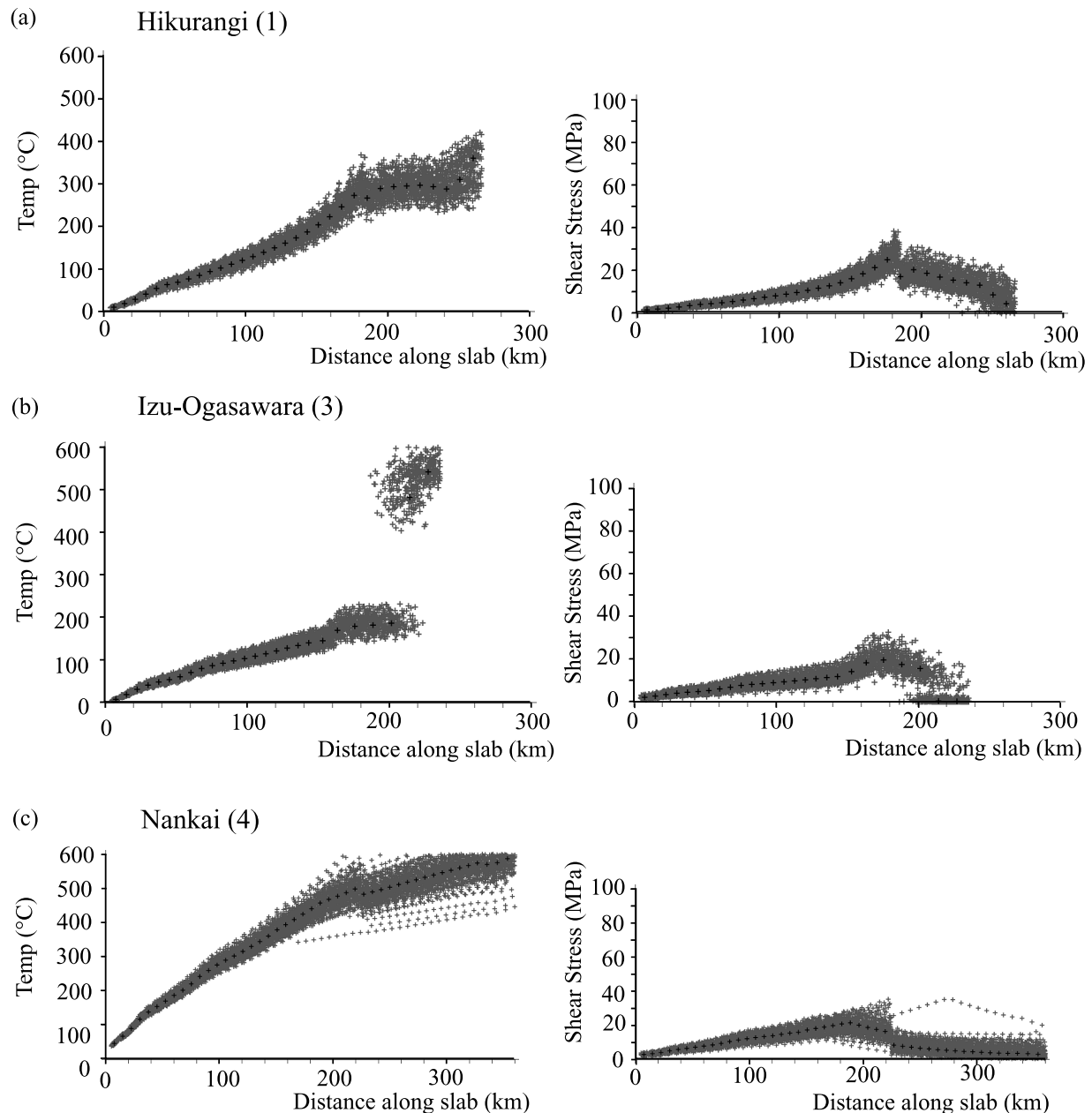
Figure 8. Plots showing Monte Carlo solutions in experiment 3 for the variation, with downdip distance along slab from trench, of temperature and shear stress along the megathrust. Black crosses show the mean solution, whereas gray crosses show possible solutions, given the uncertainty in the input parameters (see Tables 1a, 1b, 2, and 5). (a) Hikurangi subduction zone, Pacific plate subducted beneath Australian plate (location 1 in Figure 1). (b) Izu subduction zone, Pacific plate subducted beneath Philippine plate (location 3 in Figure 1). (c) Nankai subduction zone, Philippine plate subducted beneath western Japan (location 4 in Figure 1).

plate >2.5 km. More precisely, they cannot support buoyancy stress contrasts between the trench and behind arc region ≫100 MPa [*Lamb and Davis*, 2003].

[60] The ductile flow may show some sort of power law dependency (n) on strain rate. It is, however, difficult to constrain this from the A values alone, because the appropriate strain rates are unknown. If simple shear ductile flow is confined to a channel which has the same width for all subduction zones, then the strain rate might be expected to be proportional to some power of convergence velocity.

Figures 13a and 13b show log-log plots of convergence velocity against A_{crust} and A_{mantle}. The resolving power for crustal ductile behavior is very poor in the inversions, and the log-log correlation between A_{crust} and convergence velocity is weak. The best fit line has a slope (1/n) of 0.027 ($r^2 \sim 0.023$). Taken at face value, this implies high values of n (n ≫ 10). The log-log correlation between A_{mantle} and convergence velocity is also weak, but with a negative slope of −0.1025, and is therefore not consistent with a power law rheology and positive exponent n.
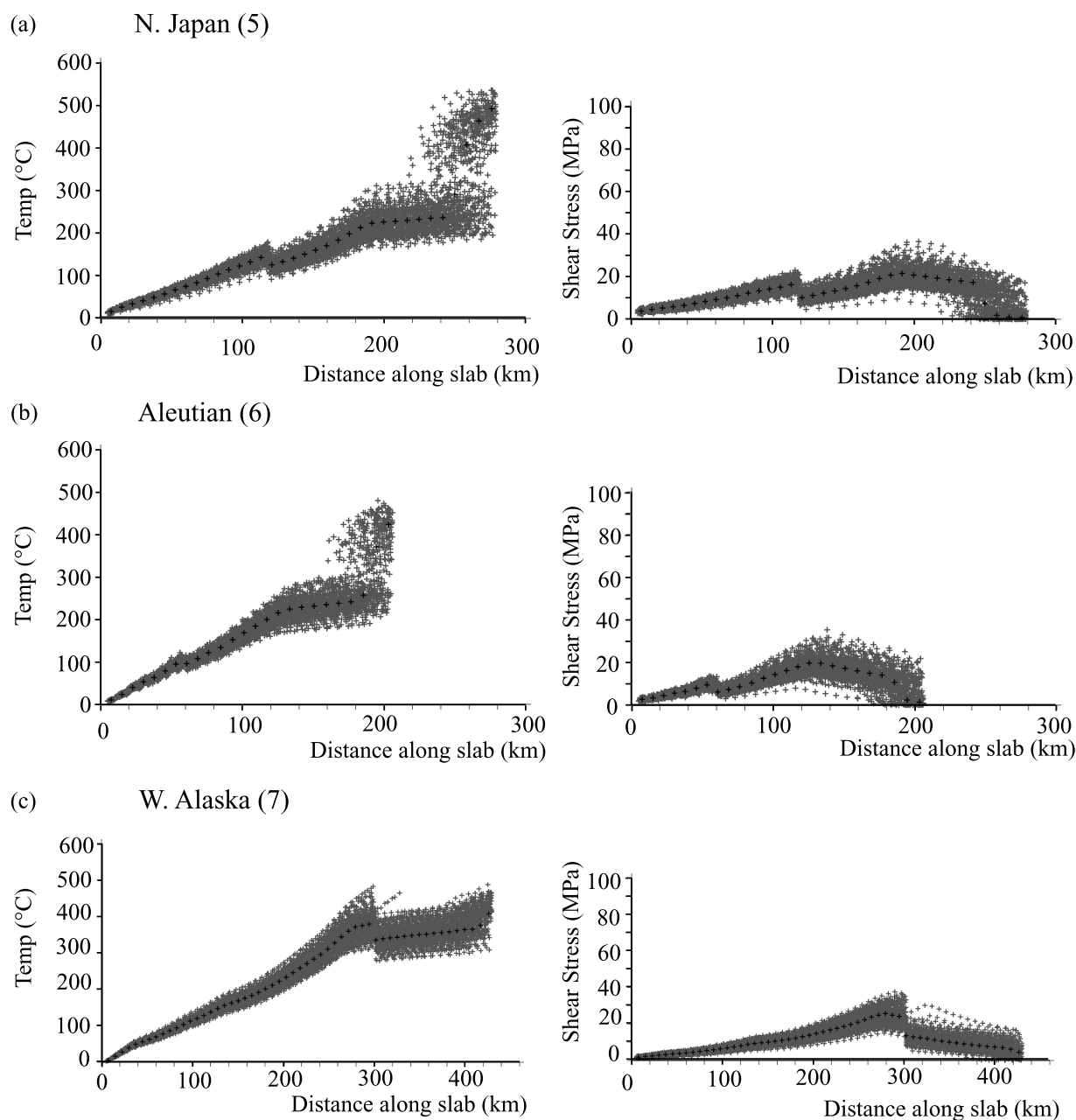
Figure 9. Plots showing Monte Carlo solutions in experiment 3 for the variation, with downdip distance along slab from trench, of temperature and shear stress along the megathrust. Black crosses show the mean solution, whereas gray crosses show possible solutions, given the uncertainty in the input parameters (see Tables 1a, 1b, 2, and 5). (a) Northern Japan subduction zone, Pacific plate subducted beneath northern Japan (location 5 in Figure 1). (b) Aleutian subduction zone, Pacific plate subducted beneath North American plate (location 6 in Figure 1). (c) Alaska subduction zone, Pacific plate subducted beneath North American plate (location 7 in Figure 1).

Removing the two hot subduction zones (Nankai and Cascadia), where the brittle-ductile transition lies well within the crust, results in virtually no log-log correlation for A_{mantle} with convergence velocity (Figure 13c, $r^2 \sim 0.0003$). These results may merely reflect the fact that the ductile channel width is not constant from subduction zone to subduction zone, possibly with a negative correlation with convergence velocity because rapidly slipping megathrusts have wider strain softened zones. In this case, the plots cannot be used to estimate reliable values of n, though there is a suggestion than n may be large.

[61] Another approach to constraining n is by assessing the activation energy. We would anticipate activation energies in the range $100-150$ kJ mol^{-1} for felsic compositions $200-250$ kJ mol^{-1} for intermediate and basic compositions and ~500 kJ mol^{-1} for ultramafic lithologies [*Ranalli*, 1995]. Given, that the rheology of the megathrust will be determined by the weakest lithologies, the crustal part
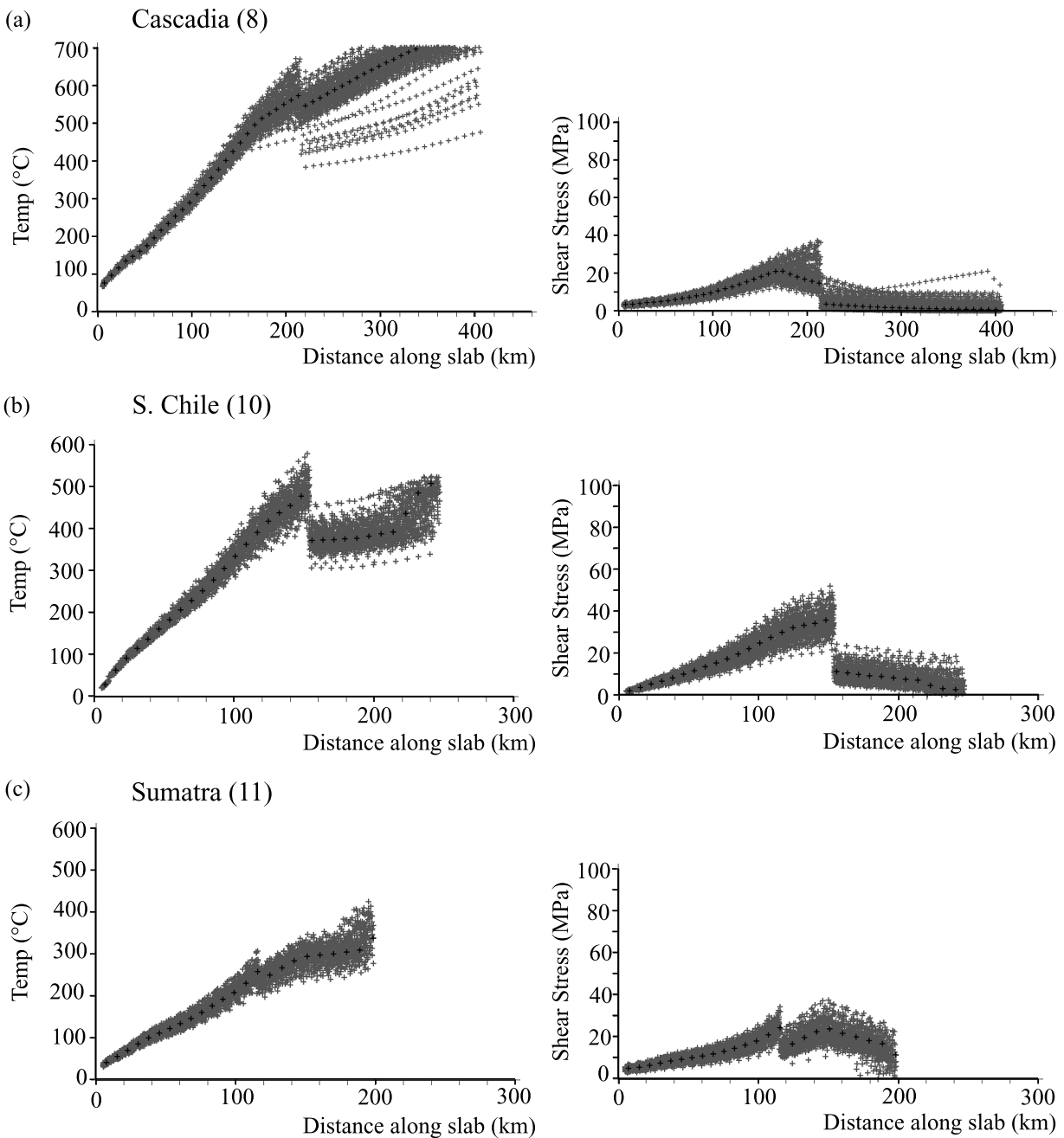
Figure 10. Plots showing Monte Carlo solutions in experiment 3 for the variation, with downdip distance along slab from trench, of temperature and shear stress along the megathrust. Black crosses show the mean solution, whereas gray crosses show possible solutions, given the uncertainty in the input parameters (see Tables 1a, 1b, 2, and 5). (a) Cascadia subduction zone, Juan de Fuca plate subducted beneath North American plate (location 8 in Figure 1). (b) Southern Chile subduction zone, Nazca plate subducted beneath South American plate (location 10 in Figure 1). (c) Sumatra subduction zone, Australian plate subducted beneath SE Asia (location 11 in Figure 1).

would be expected to have a felsic behavior, and a basic (oceanic crust) or ultramafic behavior for the mantle part. In this case, for B equaling 36 ± 18 kJ mol^{-1} (experiment 3), n would be expected to be >2 (at the 1σ confidence level) in the crustal part of the megathrust, and n > 4 (at the 1σ confidence level) in the mantle part. Given the large uncertainties in B, a maximum value for n is not well constrained, though the relatively high values for the mantle part are broadly consistent with the suggestion of large n from log-log plots of convergence velocity with A_{mantle} values (Figure 13c). However, the anticipated activation energies may not be appropriate if the ductile behavior is really a quasi-ductile effect related to subfrictional fault slip at high pore fluid pressure in high strain rate and high strain zones.
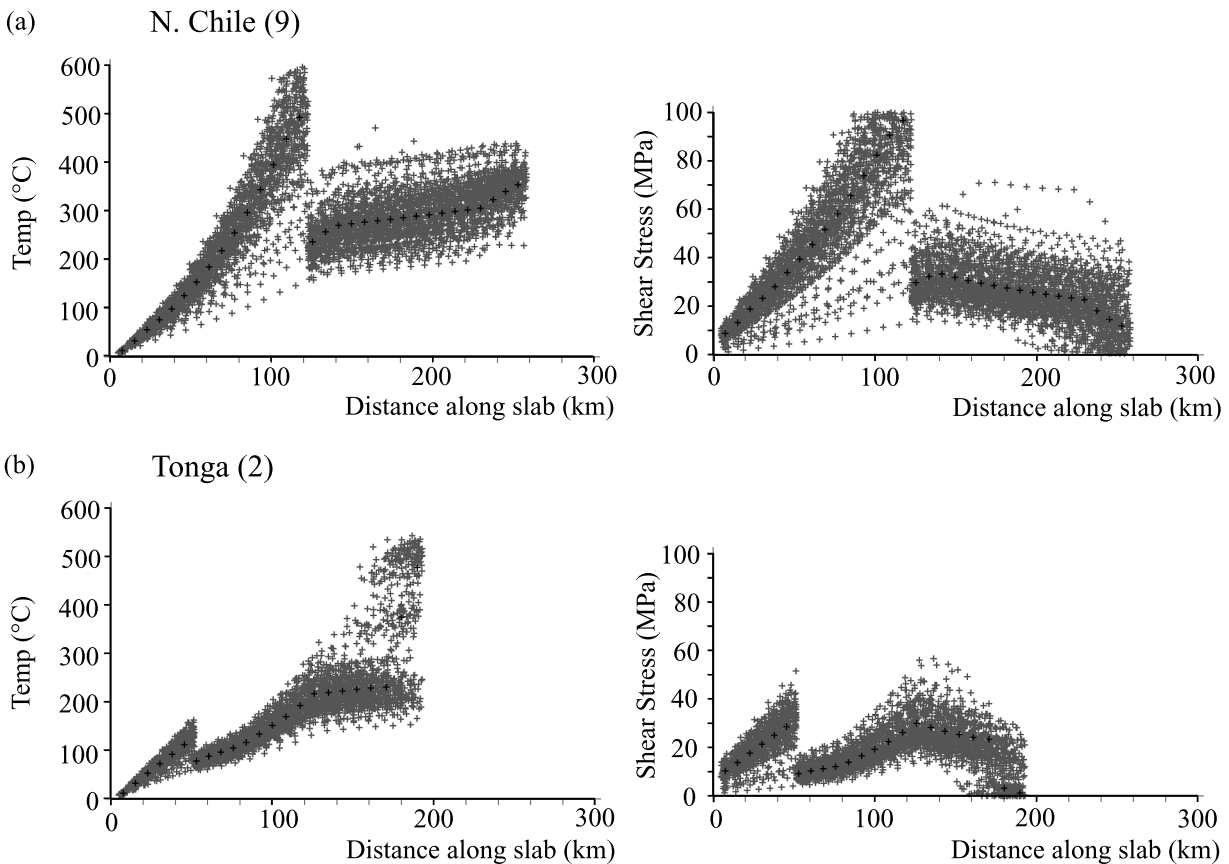
Figure 11. Plots showing Monte Carlo solutions in experiment 3 for the variation, with downdip distance along slab from trench, of temperature and shear stress along the megathrust. Black crosses show the mean solution, whereas gray crosses show possible solutions, given the uncertainty in the input parameters (see Tables 1a, 1b, 2, and 5). (a) Northern Chile subduction zone, Pacific plate subducted beneath Nazca plate (location 9 in Figure 1). (b) Tonga subduction zone, Pacific plate subducted beneath Lau Basin (location 2 in Figure 1).

6.4. Lubrication

[62] The inversions do not support the idea that average stresses on the megathrust are principally a function of the age of the subducted slab or rate of convergence; other factors such as the frictional characteristics of the megathrust in the crust and mantle must play an important role. Indeed, many subduction zones involve subduction of slabs that are older and colder than the Andean system (e.g., northeastern Japan, Izu-Ogasawara) and these do not have such large mountain ranges behind them. It would appear that something else is needed to jump the system from a "normal" low stress megathrust to an "abnormal" high stress megathrust. *Lamb and Davis* [2003] suggested that an abundant supply of trench sediment acts as a lubricant, reducing the average shear stress, because high shear stresses seem to coincide with sediment-starved trenches (<0.4 km of trench fill). In their model, trench fill smoothed out the plate interface, reducing the frictional sliding coefficient or effective viscosity and allowing easier slip. In addition, wet sediment carried deep down the megathrust raised fluid pressures, helping to reduce further frictional shear stresses (Figure 14).

[63] It is clear from the results of experiment 3 that the crustal portion of a "high" stress megathrust, such as that in

northern Chile, shows the most marked increase in effective coefficient of friction, compared to a low stress megathrust, whereas the mantle part only marginally changes. This strongly suggests that any lubrication of a megathrust by subducted sediments must be mainly confined to the crust. For this reason, the mean shear stress on a poorly lubricated megathrust will be strongly dependent on the depth of the Moho intersection. Thus the sediment-starved subduction zone in northern Chile has about double the mean shear stress (~37 MPa), compared to the sediment-starved subduction zone in Tonga (~18 MPa), because the crustal thickness on the megathrust in northern Chile is ~40 km but only is ~10 km in Tonga. In fact, because shear stresses are proportional to depth on the frictional part of a megathrust, the integrated frictional shear force in the crust will be proportional to the square of the maximum crustal thickness.

[64] It is interesting to speculate on the timescale of evolution from a low stress to high stress megathrust. If trench sediment is an important lubricant, then one would expect the timescale to be comparable to the time taken for subduction to carry sediment along the length of the megathrust. For convergence velocities in the range 40–80 mm/yr, and a megathrust length of ~200 km, one would
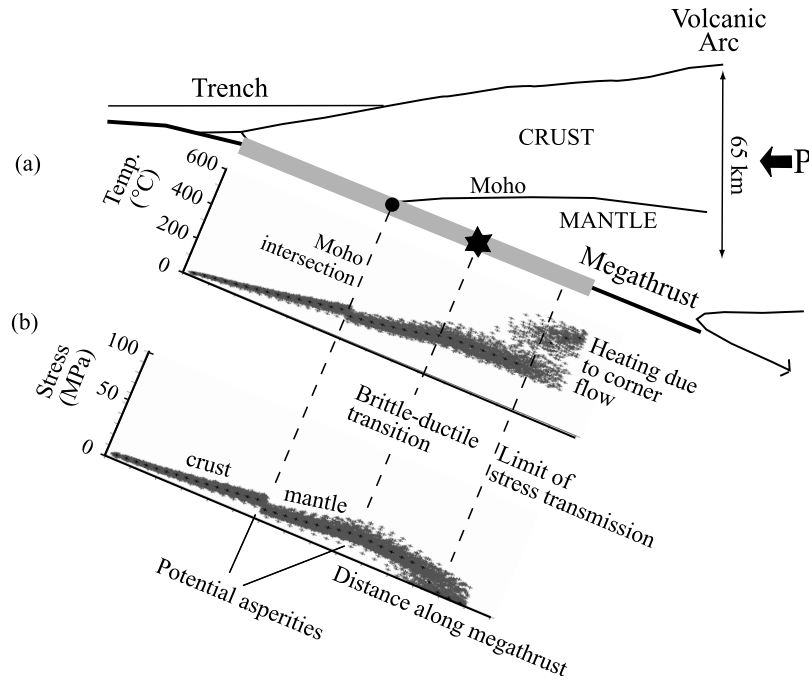
Figure 12. Diagrams illustrating the main features of temperature and shear stress along the megathrust, based on the inversion results for N. Japan in experiment 3. These results typify a "low stress" normal subduction zone, which supports maximum elevations in the highlands <2.5 km. (a) Temperature increases linearly in the brittle part, dropping slightly at the Moho, and then flattening out at the base of the seismogenic zone where T ∼ 230°C. There is a marked increase in temperature at greater depth, where the influence of the induced corner flow becomes dominant and the temperature rises to ∼500°C at the bottom of the plate interface. (b) Shear stress has a broad "hump" distribution along the megathrust, increasing linearly in the crust and brittle part of the mantle (with a drop at the Moho). Thereafter, shear stresses gradually decrease again until, at the depths near the corner flow, there is a sudden drop back to close to zero, marking the bottom end of shear stress transmission on the plate interface. Two peaks in shear stress, at the base of the crust and in the mantle at the brittle-ductile transition, could potentially act as asperities or nucleation points in great earthquakes.
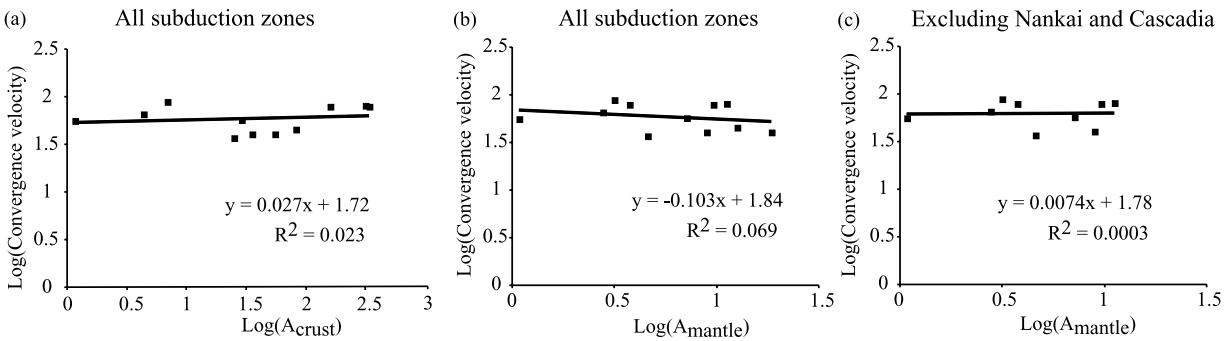

Figure 13. Log-log plots of the ductile rheological A parameter (see equation (8)) against convergence velocity, using the results of experiment 3 (Table 5). If ductile flow along the megathrust is focused into a channel of roughly constant width, then the convergence velocity will be proportional to shear strain rate (ε). For power law flow, shear stress τ will be proportional to some power of simple shear strain rate, with an exponent $1/n$. The resolving power in the inversions for the rheology of crustal ductile flow is very poor (see text). (a) Log-log plot for crustal parameter A for all subduction zones analyzed in this study. This shows a weak correlation with slope ∼0.027, suggesting large n ≫ 10. (b) Log-log plot for mantle parameter A for all subduction zones analyzed in this study. This shows a weak negative correlation with slope ∼−0.103, which is not consistent with a power law rheology and positive exponent n. (c) Log-log plot for mantle parameter A, but this time the two hot subduction zones (Nankai and Cascadia), which show significant crustal ductile flow, are excluded. This shows a very weak positive correlation with slope ∼0.0003, suggesting very large n.
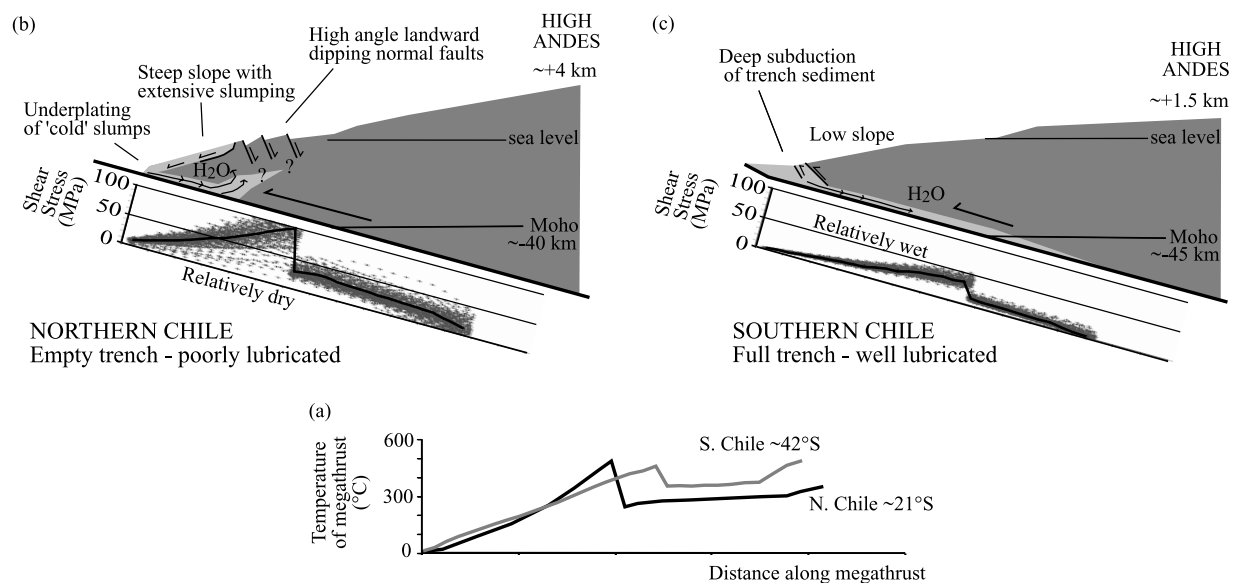
Figure 14. Diagrams illustrating the main features of temperature and shear stress along a high stress and low stress megathrust, based on the inversion results for the Peru-Chile subduction zone in northern and southern Chile in experiment 3. The presence or absence of significant trench fill could affect the process of subduction. The temperatures on the megathrust in both northern and southern Chile are similar, and for the most part within 100°C of each other, illustrated in Figure 14a. This is a consequence of the fact that the sum of the heat derived both from the subducted plate and from shear heating along the plate interface is similar for both subduction zones. Therefore the marked differences in shear stresses along the megathrusts in northern and southern Chile cannot be explained purely in terms of the thermal structure of the megathrusts but require fundamental differences in rheology, both in the crust and mantle. One possibility is that the sediment-starved trench in northern Chile, illustrated in Figure 14b, has deprived the megathrust of the lubrication that occurs in southern Chile. Extensive undermining of the toe of the sediment-starved trench in northern Chile could set up sediment "convection," where water-rich debris is dragged into the subduction zone but accumulates and rises near the up dip edge of seismogenic zone as slumping strips off the overlying prism, limiting further downdip movement of the sediment. High-angle landward dipping normal faults, typical of this type of margin, may be the coastal expression of this. Sediment full trenches, on the other hand, such as that in southern Chile, illustrated in Figure 14c, may result in "well-lubricated" and smooth subduction zones because sediment and water is dragged far down the plate interface.

expect this to be a few million years at most. If the main strength of a poorly lubricated system resides in the crust, a switch from low to high, or vice versa, could occur on an even shorter timescale (<1 Myr).

[65] Along the western margin of South America, only the central Andean portion of the subduction zone, comprising about half the total length of the Andean subduction zone, seems to have evolved as a high stress system. Although the high resistive stresses here would be expected to put a significant break on the relative motion between the Nazca and South American plates, a sufficient plate driving force must remain to maintain Andean deformation and continued convergence of the plates. The negative buoyancy of the subducted slab along the entire length of western South America may play an important role in this. Given the relative magnitudes of the various plate driving forces [*Coblenz and Richardson*, 1996], one can speculate that the development of a much greater length of the Andean subduction system as an unlubricated system could have eventually stopped plate convergence here altogether.

[66] On the foreland side of an orogenic belt, megathrusts that accommodate underthrusting of continental lithosphere may also be lubricated. This would apply to major thrusts such as those in the Himalayas or eastern margin of the Andes. For example, the average shear stress τ on a continental megathrust dipping at an angle θ beneath a triangular orogenic wedge rising to height h above the surrounding plains can be derived from equation (4):

$$\tau = \frac{\rho g h \sin 2\theta}{4} \tag{12}$$

Thus the sole thrust beneath the Himalayas, which dips on average at $10°-15°$ and supports an elevation contrast between the Tibetan plateau and the plains of India $\sim$5 km, will have an average shear stress in the range $11-17$ MPa. A comparable megathrust on the eastern margin of the central Andes would have an average shear stress $\leq$13 MPa. These results suggest that these thrusts are also low stress systems, and so, by analogy with the lubrication of subduction megathrusts, it may be sediments, either making up the deforming wedge or in the foreland basin fill, that are acting as a lubricant.
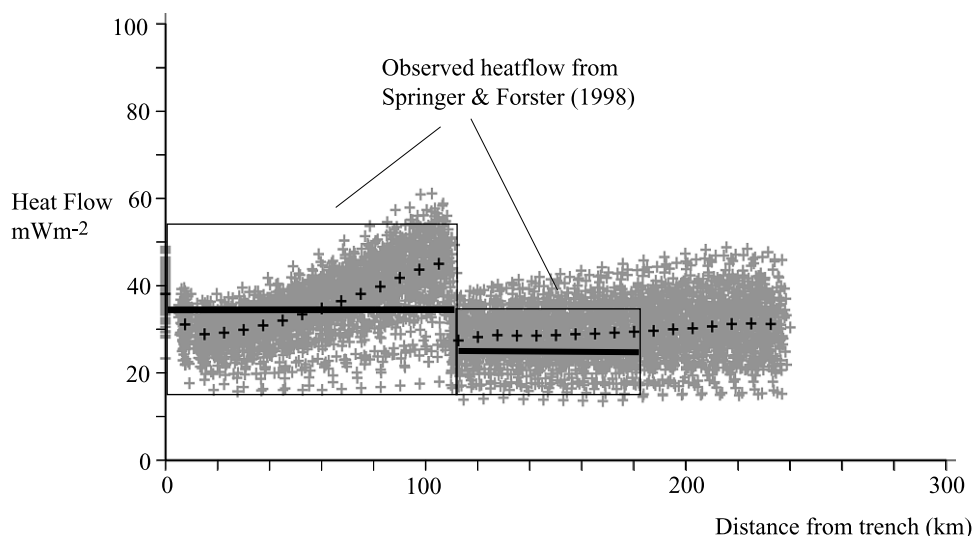
Figure 15. Diagram showing the range in calculated surface heat flow across the Andean subduction zone in northern Chile (location 9 in Figure 1), based on the results of experiment 3 (Tables 2 and 5). Black crosses show the mean solution, whereas gray crosses show possible solutions, given the uncertainty in the input parameters. Also shown are the ranges of observed heat flow measurements from *Springer and Forster* [1998], where the solid bars show the mean and the boxes show the mean absolute deviation. It is striking that the calculated marked drop in heat flow for the landward part of the subduction zone (at distances >110 km from the trench) is consistent with the low observed mean surface heat flow in this region. The drop in calculated surface heat flow occurs where the megathrust cuts the mantle. Here, the effective coefficient of friction (∼0.026) is much lower than that for the crustal part of the megathrust (∼0.095), and so there is a significant drop in the calculated amount of shear heating. Thus the observed surface heat flow measurements support the conclusion from experiment 3 that the crustal part of the megathrust is much stronger than the mantle part in northern Chile.

6.5. Lithospheric Strength

[67] The inversion results require a significant proportion of the integrated shear force on the megathrust to be transmitted both where it cuts the crust and mantle. The mantle part of the megathrust plays a particularly important role in subduction zones where the subducted slab is old (>50 Ma), and can contribute most of the integrated shear force. In hot subduction zones, where the age of the subducted slab is ≪50 Ma, almost all the stress transmission is in the crust. These results suggest that mantle rocks (or at least the lithologies along the mantle part of the megathrust) below ∼300°C have an integrated strength that is greater than or comparable to the crust. At higher temperatures, the strength of the mantle part of the megathrust becomes negligible.

[68] The megathrust in northern Chile shows a departure from this behavior, with considerable mantle strength at temperatures over 300°C. One explanation for this is that the water content of the mantle part of the megathrust is lower here. The crustal part of the megathrust here also shows significant frictional strength for temperatures >450°C, and is probably as strong as the crust can be above a subduction zone. Indeed, the rheology of the megathrust in northern Chile, with its sediment-starved trench, may be closest to the rheology of the lithosphere away from subduction zones.

[69] Surface heat flow data potentially provide an independent test of the relative magnitudes of shear stresses in the crustal and mantle parts of a megathrust. These data have not been used as a constraint in this study because of the problems in interpreting the data (see section 2.1). However, the very large predicted drop in shear stress, and hence shear heating, at the Moho intersection with the megathrust in northern Chile should show up as a significant drop in surface heat flow. It is interesting in this respect that the surface heat flow in a transect across the subduction zone in northern Chile is low (∼25 mW m^{-2}) over the coastal ranges (>110 km from the trench), in the vicinity of the Moho intersection (Figure 15) [*Springer and Forster*, 1998]. For this reason, *Springer* [1999] had difficulty modeling the surface heat flow data without assuming a low coefficient of friction on the megathrust. However, because *Springer* [1999] did not distinguish between a crustal or mantle rheology, his model required low shear stresses everywhere along the megathrust. Given the uncertainties, the surface heat flow data can be equally well fitted by high shear stresses (high coefficient of friction) in the crustal part of the megathrust, and lower shear stresses (lower coefficient of friction) in the mantle part of the megathrust, as predicted in experiment 3 (Figure 15). Indeed, the surface heat flow data here may the best available independent evidence that the shear stresses in the crustal part of an unlubricated megathrust are much higher than in the mantle, unlike the situation on lubricated megathrusts.

[70] For most subduction zones, the lithologies along the megathrust may not be representative of general mantle or crustal lithologies, but may be much "wetter" because of

the presence of a high water flux from the subducted slab. Thus subduction zones only exhibit a significant mantle strength because they are "cold" as well. In "hotter" lithosphere, the mantle could be either strong or weak depending on its water content [*Mackwell et al.*, 1998; *Hirth and Kohlstedt*, 1996].

7. Conclusions

[71] In this study, the temperatures and shear stresses along megathrusts in 11 subduction zones around the Pacific rim (Hikurangi, Tonga, Izu-Ogasawara, western Nankai, northeastern Japan, Aleutians, western Alaska, Cascadia, northern Chile, southern Chile) and SE Asia (northern Sumatra) have been determined. The main constraint is that vertical normal stresses beneath the highlands behind the subduction zone are nearly equal to horizontal normal stresses, in the plane of a trench or arc-normal section. This way, the elevations and density structure in the subduction zone can be used to constrain the integrated shear stress on the megathrust.

[72] For a megathrust with a typical brittle and ductile rheology, frictional shear stresses (τ_f) are proportional to pressure ($\tau_f = \mu \rho g z$, for depth z), and ductile shear stresses are an exponential function of temperature T ($\tau = A \exp(B/RT)$). Brittle and ductile rheological constants (μ_{crust}, μ_{mantle}, B) common to the megathrusts are determined by simultaneously solving for the force balance and thermal structure, using a multiple restart Monte Carlo simplex minimization algorithm, taking account of the induced mantle corner flow at depth (65 ± 15 km (2σ)) and constant radiogenic heating (0.65 ± 0.3 μW m^{-3} (2σ)) throughout the crust. The A constants were solved individually for each subduction zone, assuming that the maximum depth of interplate slip earthquakes marks the brittle-ductile transition. The results are as follows:

[73] 1. The best fit solution shows two groupings of megathrusts, with most subduction zones having a mean shear stress in the range 7–15 MPa ($\mu_{crust} = 0.032 \pm 0.006$, $\mu_{mantle} = 0.019 \pm 0.004$), and are unable to support elevations >2.5 km. The low effective coefficients of friction suggest high pore fluid pressures at ~95% lithostatic pressure, for a typical frictional sliding coefficient of 0.5. For Tonga and northern Chile, $\mu_{crust} = 0.095 \pm 0.024$, $\mu_{mantle} = 0.026 \pm 0.007$, suggesting slightly lower pore fluid pressures, at ~81% lithostatic in the crust, compared to the other grouping.

[74] 2. Ductile shear in the crust is poorly resolved but in the mantle appears to show a strong power law dependency, with B = 36 ± 18 kJ mol^{-1}. A_{mantle} values are sensitive to the precise value of B, but are in the range 1–20 kPa. The power law exponent n for mantle flow is poorly constrained but is likely to be large (n > 4).

[75] 3. The brittle-ductile transition in the crust occurs at temperatures in the range 370°C–512°C, usually close to the base of the crust, and in the mantle at much lower temperatures (180°C–300°C). The low temperatures in the mantle for the onset of ductile behavior could suggest that the transition in the mantle really reflects a marked change in pore fluid pressure or quasi ductile and subfrictional properties.

[76] 4. In subduction zones where the subducted slab is older than 50 Ma, a significant proportion of the integrated shear force on the megathrust is taken up where it cuts the mantle and mantle temperatures are <300°C. In younger subduction zones, the stress transmission is mainly confined to the crust.

[77] 5. The megathrust in northern Chile has a mean shear stress ~37 MPa, necessary to support elevations >4 km in the high Andes. Such a high stress system cannot be explained in terms of the thermal structure, or high strain rate, but requires either lower pore fluid pressures or different fundamental rheological constants, especially in the crust.

[78] 6. The inversion results support the suggestion that shear stresses on the frictional part of the megathrust, particularly in the crust, are kept low by some sort of lubricant [*Lamb and Davis*, 2003]. The most plausible lubricant is the water-rich trench fill, typical of normal low stress subduction zones. Sediment may also act as a lubricant on megathrusts accommodating underthrusting of continental crust, such as in the Himalayas or eastern central Andes, which also appear to be low stress systems with mean shear stresses in the range 11–17 MPa. The absence of a lubricant may be an important factor in changing the megathrust rheology, lowering pore fluid pressure and creating a rougher plate interface, so that the subduction zone becomes an abnormal high stress system, capable of supporting elevations such as those in the Andes. However, where the crust is thin in a sediment-starved and poorly lubricated subduction system, such as Tonga, the mean shear stress will still be low.

Appendix A

A1. Minimization Algorithm

[79] The aim is to search for the set of rheological constants in equations (7) and (8) that are common to a number of subduction zones, subject to a set of constraints (see main text).

[80] The inversion procedure is carried out using a downhill simplex algorithm [*Press et al.*, 1992] called Amoeba. For each trial set of rheological constants, the function F(μ, A, B) is evaluated, summed over the number of subduction zones N:

$$F(\mu, A, B) = \sum_{N} (P_{obs} - P_{calc})^2 \qquad (A1)$$

where for each subduction zone, P_{obs} is the observed push at the back of the wedge, from equation (5), and P_{calc} is the calculated from the integration of megathrust shear stresses, given a set of rheological parameters and density structure of the wedge. A positivity constraint is imposed on μ.

[81] The downhill simplex algorithm searches for a set of rheological constants, common to all the subduction zones, that minimize F(μ, A, B). The simplex is initiated with an arbitrary set of constants, and F(μ, A, B) is then evaluated by solving for the shear stress and temperature distributions that satisfy equations (7)–(12) and equations (A4)–(A6) (corner flow thermal structure). Shear stress and temperature is determined at constant horizontal increments along the megathrust, using a Newton-Raphson iteration to satisfy equations (8), (10), and (12) simultaneously.
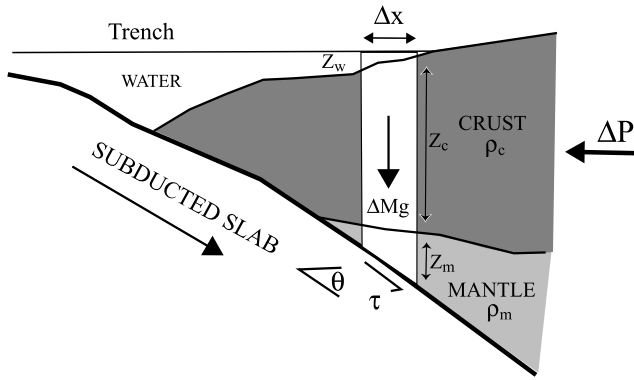
Figure A1. Diagram illustrating procedure for calculating the force balance along a curved megathrust, locally dipping at angle θ. A column, with width Δx, has a basal shear stress τ and an internal body force ΔMg, per unit arc length. The resolved sum of these forces must be balanced by the horizontal push ΔP per unit arc length ($\Delta P = \Delta Mg \tan\theta + \tau \Delta x / \cos^2\theta$), where the mass ΔM per unit arc length is determined by the local crustal and mantle structure ($\Delta M = \Delta x \, (\rho_w z_w + \rho_c z_c + \rho_m z_m)$). The basal shear stress in each column is a function of the rheology of the megathrust and the PT conditions at the base of the column. The sum of all the increments of push must balance the total push P at the back of the subduction wedge.

[82] In practice, it was found that there are numerous local minima in $F(\mu, A, B)$. The global minimum was found by restarting the algorithm with a wide range of starting conditions. In addition, local minima are screened by only accepting solutions with fits below a set threshold value. Uncertainties in the solutions were determined using a Monte Carlo technique, running multiple realizations of the input data (crustal and density structure of wedge, depth of the base of seismogenic zone, increments at which stresses and temperatures are evaluated, heat flow from subducted slab, convergence velocity in subduction zone, thermal parameters, push at back of wedge etc.), by randomly perturbing them within their own uncertainty ranges. The mean and standard deviation of the solutions that yield a global minimum of $F(\mu, A, B)$, for a large number of realizations of the data, are the best estimates of the rheological constants and their uncertainties, given the model and data.

[83] The overall minimization procedure is expensive on computer time because it involves an iteration of both the simplex starting conditions and the values of the input data, and an iteration in the simplex algorithm itself. The program was written by the author in Fortran, and a typical run on a Sun Sparc station takes about an hour.

A2. Curved Megathrust

[84] The force balance analysis presented in equations (2)–(4) assumes a planar megathrust with a constant dip. In reality, Benioff zones are curved and so the dip of the megathrust will vary, generally increasing with depth. For this situation, the force balance equation has to be integrated across the overlying wedge. If we neglect all vertical shear forces within the wedge (in effect, assume negligible flexural strength), then we can determine the increment of push ΔP

for any vertical crustal column (per unit arc length), with mass ΔM and width Δx, in the wedge (Figure A1):

$$\Delta M = \Delta x (\rho_w z_w + \rho_c z_c + \rho_m z_m),$$

$$\Delta P = \Delta Mg \tan\theta + \tau_s \left(\frac{\Delta x}{\cos^2\theta} \right) \qquad (A2)$$

where τ_s and θ are the local shear stress and dip of the megathrust at the base of the column, and the mass depends on the local wedge density structure. The actual value of τ_s is defined by equations (7), (8), and (10).

A3. Density Contrasts

[85] The mass of the wedge can be determined from its density structure. For the subduction zones considered (Table 1a), the crustal structure is relatively well constrained. However, the actual densities are more difficult to determine. In principle, they could be extracted from high-quality refraction surveys, using an appropriate velocity-density relation, though there may be significant uncertainty about whether or not the P wave velocity is also a strong function of other rock properties such as water content. In fact, the important parameter is the density contrast between the crust in the wedge and the crust in the region behind the wedge. In general, refraction studies show that the density decreases both upward and toward the trench, where there is more accreted material in the wedge. For the typical range of seismic velocities in the wedge (P wave velocities in the range 4–7 km s^{-1}), the mean wedge crustal density will be between 0.05 and 0.15 g cm^{-3} less than that in the crust behind the wedge (Table 1b); seismic velocities (P wave velocity $\sim$8 km s^{-1}) suggest that the mantle densities will be in the range 3.25–3.3 g cm^{-3}.

A4. Average Thermal Conductivity in Prism Above Megathrust

[86] The average thermal conductivity in the prism above the megathrust will depend on the crustal and mantle structure of the prism [*Tichelaar and Ruff*, 1993]. For a megathrust at depth z_f, with an overlying crustal thickness z_c, and crustal thermal conductivity k_c, and mantle thickness and thermal conductivity of z_m and k_m, respectively, the average thermal conductivity k is given by

$$k = \frac{z_f}{\left(\dfrac{z_c}{k_c} + \dfrac{z_m}{k_m} \right)} \qquad (A3)$$

A5. Evaluation of Temperatures Near the Mantle Corner Flow

[87] *England and Wilkins* [2004] show that where there is a corner flow in the mantle wedge above the subducted slab (thickness a, dipping at angle θ, and sliding into the mantle at velocity V), the temperature at the top of the subducted slab, at a depth z, is approximately given by the following expression, for a corner flow starting at depth z_L (thickness of overriding plate):

$$T \approx \left(T_1 + \frac{\sqrt{\pi}\alpha T_a}{2a} erf\left(\frac{a}{2\sqrt{\kappa t}} \right) \right) / \left(1 + \frac{\sqrt{\pi}\alpha}{2\beta} \right) \qquad (A4)$$

where

$$\frac{\sqrt{\pi}\alpha}{2a} = \left(\frac{2\pi}{9\xi}\right)^{\frac{1}{3}}\left(1 - \frac{z_L}{z}\right)\left(\frac{V\theta^2 r}{\kappa}\right)^{\frac{1}{6}}$$

$$\left(\frac{2\pi}{9\xi}\right)^{\frac{1}{3}} \approx 0.85$$

$$\beta = \sqrt{kz/v\sin\theta}$$

T_1 is the local maximum temperature in the corner flow, and T_a is the reference mantle temperature (taken as 1280°C). For subducted slabs older than 50 Ma, the temperature to good approximation is simply

$$T \approx T_1 / \left(1 + \frac{\sqrt{\pi}\alpha}{2\beta}\right) \qquad (A5)$$

The maximum temperature in the corner flow (T_1), for distance r along the top of the subducted slab from the corner (at depth z_L), is given to good approximation by

$$T_1 \approx T_a \exp\left(0.5\left[1 - \left(\frac{R}{r}\right)^{\frac{1}{3}}\right]\right) \qquad (A6)$$

where

$$R = \frac{400\kappa}{V\theta^2}$$

The temperature structure along the megathrust is defined by equation (10) for depths $<z_L$. For depths $>z_L$, the temperature on the slab is taken to be the larger of either the temperature defined by equation (10) or (A5). Generally, the corner flow temperature is significantly higher at depths 10 km or deeper than z_L.

A6. Temperature Discontinuities Along Megathrust

[88] The thermal structure for the megathrust at shallower depths than the corner flow assumes that heat flow in the lithospheric wedge is vertical. Given that the average dip of the megathrust is $<20°$, this is generally likely to be a good approximation. However, where there are sudden jumps in the shear stress on the megathrust, usually at the crust-mantle boundary, this approximation gives rise to temperature discontinuities. In reality, such marked changes in temperature along the megathrust would be more smoothed out by lateral heat flow. Nonetheless, the more regional thermal structure is unlikely to be significantly different because the megathrust is inclined at such a shallow angle.

[89] For example, a marked temperature jump of 100°C over a distance of 20 km down the length of the megathrust translates into a temperature gradient of ~5°C/km, compared to a typical vertical temperature gradient in the overlying lithospheric wedge of ~10°C/km. Thus, even where heat generation due to shear heating changes markedly along the megathrust, vertical heat flow will still dominate.

A7. Obliquity of Megathrust Slip Vector

[90] If the megathrust is not a pure thrust, than some allowance must be made for the obliquity of slip in both the

force balance and thermal structure (Table 1a). The shear stress is simply resolved into the downdip direction of shear by a factor cos φ, where φ is the obliquity of megathrust slip (φ = 0 is pure thrust).

[91] The thermal equations (equations (1), (10), and (A4)–(A6)) contain the convergence velocity V. The velocity V in the advection factor S (equation (1)), and the velocity in the corner flow equations (equations (A4)–(A6)), refers to the dip slip component of velocity which is carrying material downward. However, the velocity in the shear heating equation (equation (10)) is the full velocity of interplate shearing that is generating heat.

[92] For the subduction zones analyzed in this study, φ is $<20°$ because the relative plate convergence is either nearly orthogonal to the trench, or where it is significantly oblique (e.g., Hikurangi and Sumatra), there is strike-slip behind the subduction zone, so that relative motion on the megathrust remains nearly dip slip. Thus any correction for oblique slip in this study is small $<6\%$.

References

Angermann, D., J. Klotz, and C. Reigber (1999), Space-geodetic estimation of the Nazca–South America Euler vector, *Earth Planet. Sci. Lett.*, *171*, 329–334.

Asch, G., et al. (2003), Seismic imaging of a convergent continental margin and plateau in the central Andes (Andean Continental Research Project 1996 (ANCORP'96)), *J. Geophys. Res.*, *108*(B7), 2328, doi:10.1029/2002JB001771.

Bishop, A. W., G. E. Green, V. K. Garga, A. Andresen, and J. D. Brown (1971), A new ring shear apparatus and its application to the measurement of residual shear strength, *Geotectonique*, *21*, 273–328.

Bourne, S. (1996), Distributed deformation of the South Island of New Zealand, Ph.D. thesis, 188 pp., Univ. of Oxford, Oxford, U. K.

Cartwright, J. A., and L. Lonergan (1996), Volumetric contraction during the compaction of mudrocks: A mechanism for the development of regional scale polygonal fault systems, *Basin Res.*, *8*, 183–193.

Coblenz, D., and R. M. Richardson (1996), Analysis of the South American intraplate stress field, *J. Geophys. Res.*, *101*, 8643–8657.

DeMets, C., R. G. Gordon, D. F. Argus, and S. Stein (1994), Effect of recent revisions on to the geomagnetic reversal time scale on estimates of current plate motions, *Geophys. Res. Lett.*, *21*, 2191–2194.

England, P. C., and G. Houseman (1986), Finite strain calculations of continental deformation: 2. Comparison with the India-Asia collision zone, *J. Geopys. Res.*, *91*, 3664–3676.

England, P. C., and D. P. McKenzie (1982), A thin viscous sheet model for continental deformation, *Geophys. J. R. Astron. Soc.*, *70*, 295–321. (Correction to "A thin viscous sheet model for continental deformation," *Geophys. J. R. Astron. Soc.*, *73*, 523–532, 1983.)

England, P. C., and P. Molnar (1997), Active deformation of Asia: From kinematics to dynamics, *Science*, *278*, 647–649.

England, P. C., and C. Wilkins (2004), A simple analytical approximation to the temperature structure of subduction zones, *Geophys., J. Int.*, *159*, 1138–1154.

England, P. C., R. Engdahl, and W. Thatcher (2004), Systematic variation in the depths of slabs beneath arc volcanoes, *Geophys. J. Int.*, *156*, 377–408.

GEBCO (2003), Intergovernmental Oceanographic Commission (IOC), GEBCO 1-minute grid [CD-ROM], UNESCO, Paris. (Available at http://www.ngdc.noaa.gov/mgg/gebco/)

Hall, L. (2003), Cenozoic deformation at the southern end of the Hikurangi Margin, New Zealand, Ph.D. thesis, 293 pp., Univ. of Oxford, Oxford, U. K.

Hirth, G., and D. L. Kohlstedt (1996), Water in the oceanic upper mantle: Implications for rheology, melt extraction and the evolution of the lithosphere, *Earth Planet. Sci. Lett.*, *144*, 93–108.

Holbrook, W. S., D. Lizarralde, S. McGeary, N. Bangs, and J. Deibold (1999), Structure and composition of the Aleutian island arc and implications for continental growth, *Geology*, *27*, 31–34.

Houseman, G. A., and P. C. England (1986), Finite strain calculations of continental deformation: 1. Method and general results for convergent zones, *J. Geophys. Res.*, *91*, 3651–3663.

Husson, L., and Y. Ricard (2004), Stress balance above subduction: Application to the Andes, *Earth Planet. Sci. Lett.*, *222*, 1037–1050.

Hyndman, R. D., and K. Wang (1993), Thermal constraints on the zone of major thrust earthquake failure: The Cascadia Subduction Zone, *J. Geophys. Res.*, *98*, 2039–2060.

Jackson, J. A. (2002), Strength of the continental lithosphere: Time to abandon the jelly sandwich?, *GSA Today*, *12*(9), 4–9.

Kodaira, S., et al. (2000), Western Nankai Trough seismogenic zone: Results from a wide-angle ocean bottom survey, *J. Geophys. Res.*, *105*, 5887–5905.

Lallemand, S. E., P. Schnurle, and J. Malavieille (1994), Coulomb theory applied to accretionary and non-accretionary wedges: Possible causes for tectonic erosion and/or frontal accretion, *J. Geophys. Res.*, *99*, 12,033–12,055.

Lamb, S. H. (1987), A model for tectonic rotation about a vertical axis, *Earth Planet. Sci. Lett.*, *84*, 75–86.

Lamb, S. H. (1994), Behavior of the brittle crust in wide zones of deformation, *J. Geophys. Res.*, *99*, 4457–4483.

Lamb, S. H. (2000), Active deformation in the Bolivian Andes, South America, *J. Geophys. Res.*, *105*, 25,627–25,653.

Lamb, S. H. (2002), Is it all in the crust?, *Nature*, *420*, 130–131.

Lamb, S. H., and P. Davis (2003), Cenozoic climate change as a possible cause for the rise of the Andes, *Nature*, *425*, 792–797.

Mackwell, S. J., M. E. Zimmerman, and D. L. Kohlstedt (1998), High temperature deformation of dry diabase with application to tectonics on Venus, *J. Geophys. Res.*, *103*, 975–984.

Maggi, A., J. A. Jackson, D. McKenzie, and K. Priestley (2000a), Earthquakes focal depths, effective elastic thickness, and the strength of the continental lithosphere, *Geophys. J. Int.*, *143*, 629–661.

Maggi, A., J. A. Jackson, K. Priestley, and C. Baker (2000b), A re-assessment of focal depth distributions in southern Iran, the Tien Shan and northern India: Do earthquakes occur in the continental mantle?, *Geology*, *28*, 495–498.

McKenzie, D. P., and D. Fairhead (1997), Estimates of the effective elastic thickness of the continental lithosphere from Bouguer and free-air gravity anomalies, *J. Geophys. Res.*, *102*, 27,523–27,552.

McKenzie, D. P., and J. A. Jackson (1983), The relationship between strain rates, crustal thickening, paleomagnetism, finite strain and fault movements within a deforming zone, *Earth. Planet. Sci. Lett.*, *65*, 182–202.

Menke, W. (1988), *Geophysical Data Analysis: Discrete Inverse Theory*, *Int. Geophys. Ser.*, vol. 45, Elsevier, New York.

Molnar, P., and P. England (1990), Temperatures, heat flux, and frictional stress near major thrust faults, *J. Geophys. Res.*, *95*, 4833–4856.

Moore, J. C., et al. (1991), EDGE deep seismic reflection transect of the eastern Aleutian arc-trench layered lower crust reveals underplating and continental growth, *Geology*, *19*, 420–424.

Muller, R. D., W. R. Roest, J.-Y. Royer, L. M. Gahagan, and J. G. Sclater (1997), Digital isochrons of the world's ocean floor, *J. Geophys. Res.*, *102*, 3211–3214.

National Earthquake Information Center (NEIC) (2003), *Earthquake Catalogue*, World Data Centre for Seismol., U.S. Geol. Surv., Denver, Colo.

Parsons, B., and J. G. Sclater (1977), An analysis of the variation of ocean floor bathymetry and heat flow with age, *J. Geophys. Res.*, *82*, 803–827.

Parsons, T., A. M. Trehu, J. H. Leutgart, K. Miller, F. Kilbride, R. E. Wells, M. A. Fisher, E. Flueh, U. S. ten Brink, and N. I. Christiansen (1998), A new view into Cascadia subduction zone and volcanic arc: Implications for earthquake hazards along the Washington margin, *Geology*, *26*, 199–202.

Peacock, S. M. (1996), Thermal and petrologic structure of subduction zones, in *Subduction, Top to Bottom*, *Geophs. Monogr. Ser.*, vol. 96, edited by G. E. Bebout et al., pp. 119–133, AGU, Washington, D. C.

Press, W. H., S. A. Teukolsky, W. T. Vetterling, and B. P. Flannery (1992), *Numerical Recipes in FORTRAN 77*, 2nd ed., Cambridge Univ. Press, New York.

Ranalli, G. (1995), *Rheology of the Earth*, 2nd ed., CRC Press, Boca Raton, Fla.

Richardson, R. M., and D. Coblenz (1994), Constraint on intraplate stress magnitudes from stress modeling in the Andes of South America, *J. Geophys. Res.*, *99*, 22,015–22,025.

Simones, M., J. P. Avouac, R. Cattin, and P. Henry (2004), The Sumatra subduction zone: A case for a locked fault zone extending into the mantle, *J. Geophys. Res.*, *109*, B10402, doi:10.1029/2003JB002958.

Smith, A. G. (1981), Subduction and coeval thrust belts, with particular reference to North America, in *Thrust and Nappe Tectonics*, edited by K. R. McClay and N. J. Price, *Geol. Soc. Spec. Publ.*, *9*, 111–124.

Springer, M. (1999), Interpretation of the heat-flow density in the central Andes, *Tectonophysics*, *306*, 377–395.

Springer, M., and A. Forster (1998), Heat-flow density across the central Andean subduction zone, *Tectonophysics*, *291*, 123–139.

Stern, T. A., and F. J. Davey (1989), Crustal structure and origin of basins formed behind the Hikurangi subduction zone, New Zealand, in *Origin and Evolution of Sedimentary Basins and Their Energy and Mineral Resources*, *Geophys. Monogr. Ser.*, vol. 48, edited by R. A. Price, pp. 73–85, AGU, Washington, D. C.

Suyehiro, K., N. Takahashi, Y. Ariie, Y. Yokoi, R. Hino, M. Shinohara, T. Kanazawa, N. Hirata, H. Tokuyama, and A. Taira (1996), Continental crust, crustal underplating, and low-Q upper mantle beneath an oceanic island arc, *Science*, *272*, 390–392.

Takahashi, N., et al. (2004), Seismic structure and seismogenesis off Sanriku region, northeastern Japan, *Geophys. J. Int.*, *159*, 129–145.

Tichelaar, B. W., and L. J. Ruff (1993), Depth of seismic coupling along subduction zones, *J. Geophys. Res.*, *98*, 2017–2037.

von Huene, R., and D. W. Scholl (1991), Observations at convergent margins concerning sediment subduction, subduction erosion, and the growth of continental crust, *Rev. Geophys.*, *29*, 279–316.

Watts, A. B. (2001), *Isostasy and Flexure of the Lithosphere*, Cambridge Univ. Press, New York.

Wdowinski, S., and Y. Bock (1994), The evolution of deformation and topography of high elevated plateaus: 1. Model, numerical analysis, and general results, *J. Geophys. Res.*, *99*, 7103–7119.

―――――――――――――

S. Lamb, Department of Earth Sciences, University of Oxford, Parks Road, Oxford OX1 3PR, UK. (simon.lamb@earth.ox.ac.uk)